

Southeastern Arabian Sea Salinity variability: mechanisms and influence on surface temperature

V.P. Akhil*¹, M. Lengaigne², K. S. Krishnamohan³, M. G. Keerthi⁴, J. Vialard⁴

¹CSIR-National Institute of Oceanography, Physical Oceanography Division, Dona Paula, India.

²MARBEC, University of Montpellier, CNRS, IFREMER, IRD, Sete, France

³School of Environmental Studies, Cochin University of Science and Technology, Cochin, India

⁴LOCEAN-IPSL, Sorbonne Universités-CNRS-IRD-MNHN, Paris, France

3rd Submission to *Climate Dynamics*

*Corresponding author: V.P. Akhil (akhil@nio.org)

ORCID id: 0000-0002-8878-1053

Abstract

Previous studies suggest that the winter surface freshening in the south-eastern Arabian Sea (SEAS) contributes to the development of very high Sea Surface Temperatures (SST) thereby influencing the following summer monsoon onset. Here, we use forced and coupled simulations with a regional ocean general circulation model to explore the SEAS Sea Surface Salinity (SSS) variability mechanisms and impact on the monsoon. Both configurations capture the main SEAS oceanographic features, and confirm that the winter SSS decrease results from horizontal advection of Bay of Bengal freshwater by the cyclonic circulation around India during fall. A coupled model sensitivity experiment where salinity has no effect on mixing indicates that the salinity stratification reduces the SEAS mixed layer cooling by vertical processes by 3°C seasonally. Salinity however enhances mixed layer cooling by a similar amount through concentrating negative winter surface heat fluxes into a thinner mixed layer, resulting in no climatological impact on SST and summer monsoon rainfall. The Indian Ocean Dipole (IOD) is the main driver of the winter SEAS SSS interannual variability ($r \sim 0.8$). Salty anomalies generated in the western Bay of Bengal during fall by positive IOD events are indeed transported by the cyclonic climatological coastal circulation, reaching the SEAS in winter. By this time, warm IOD-induced SST anomalies in the SEAS are already decaying, and the SEAS SSS anomalies hence do not contribute to their development. Overall, our model results suggest a weak climatological and interannual impact of the SEAS winter freshening on local SST and following monsoon onset.

Keywords: South-eastern Arabian Sea, Sea surface salinity, Sea surface temperature, Indian Ocean Dipole, Summer monsoon, Interannual variability

1. Introduction

The south-eastern Arabian Sea (SEAS) has some of the warmest Sea Surface Temperatures (SSTs) in the world, exceeding 30°C in April-May, the months preceding the onset of the Indian summer monsoon (Seetaramayya and Master, 1984; Shenoi et al. 1999; Rao and Sivakumar, 1999; Sengupta et al. 2002). The SSTs of this so-called “Arabian Sea mini Warm Pool” (hereafter ASWP) are well above the minimum threshold ($\sim 28^{\circ}\text{C}$) for deep atmospheric convection to occur (Gadgil et al. 1984). Thus, this warm pool is thought to play an important role in the formation of the monsoon onset vortex (Shenoi et al. 1999; Rao and Sivakumar, 1999; Deepa et al. 2007; Vinayachandran et al. 2007) and in the onset of the Indian summer monsoon (Kershaw, 1985, 1988; Masson et al. 2005; Neema et al. 2012; Chacko et al. 2012).

Given its potential importance to regional climate, the seasonal evolution of the ASWP has been extensively studied from observations (e.g., Shenoi et al. 1999; Rao and Sivakumar, 1999, 2003) and ocean simulations (e.g., Durand et al. 2004, 2007; Kurian and Vinayachandran, 2007; Nyadjro et al. 2012). A freshening of the upper ocean in December-January (Fig. 1b) precedes the formation of the ASWP in April-May (Fig. 1a) (e.g., Prasanna Kumar et al. 2004; Gopalakrishna et al. 2005; Nyadjro et al. 2012). This drop in Sea Surface Salinity (SSS) has been attributed to horizontal advection of freshwaters from the Bay of Bengal (BoB) (e.g., Rao and Sivakumar, 2003; Nyadjro et al. 2012). The coastal currents around India are indeed cyclonic in winter, with a southward-flowing East India Coastal Current (EICC) in the BoB, westward-flowing Northeast Monsoon Current (NMC) near the South Indian tip, and northward-flowing West India Coastal Current (WICC) in the SEAS. This forms a continuous circulation pathway that exports about 14% of the excess freshwater received by the BoB during the southwest monsoon to the SEAS (Fig. 13a of Chaitanya et al. 2021). This winter circulation pattern is partly established by a coastal downwelling Kelvin wave that is forced by a combination of local winds and upstream wind variations in the BoB (e.g., Shankar and Shetye, 1997; Fig. 1c,d) and near the southern tip of India (Suresh et al. 2016). This downwelling signal propagates westward under the form of Rossby waves, resulting in the formation of the Laccadive (or Lakshadweep) high in the SEAS (e.g., Shankar and Shetye, 1997). Combined with the arrival of fresh and relatively cold surface waters, this leads to the formation of a thick barrier layer (Fig. 1e) between the base of the shallow salinity-controlled mixed layer (Fig. 1f) and the top of the thermocline (Durand et al. 2007; Thadathil et al. 2008). Such a layer can influence the evolution of SST, because the salinity-stratified layer prevents cooling through vertical mixing by isolating the surface layer from deeper colder water: it is therefore generally referred to as “barrier layer” (Lukas and Lindström, 1991). In the SEAS, salinity stratification in the

barrier layer is even strong enough to support persistent temperature inversions, which can lead to an unusual situation of entrainment warming (Thadathil and Gosh, 1992; Durand et al. 2004; Gopalakrishna et al. 2005). While most previous studies agree that local atmospheric forcing is the dominant driver of the ASWP formation (Rao and Sivakumar, 1999; Durand et al. 2004; Kurian and Vinayachandran, 2007; Nyadjro et al. 2012), some studies argue that salinity stratification also contributes by re-injecting the heat trapped in the barrier layer into the mixed layer from November to March (Durand et al. 2004; Masson et al. 2005; Nyadjro et al. 2012). The influence of the SEAS freshening on the ASWP is however still debated. Some modelling studies indeed argue that the SEAS freshening contributes to an early warming (Durand et al. 2004; Hareesh Kumar et al. 2009) and influences the monsoon onset (Masson et al. 2005, Nyadjro et al. 2012), while others suggest that this contribution is negligible (Kurian and Vinayachandran, 2007).

Beyond seasonal variations, ASWP warming also experiences significant interannual variations (Rao and Goswami, 1988; Subrahmanyam et al. 2011; Nyadjro et al. 2012; Rao et al. 2015; Rao and Ramakrishan, 2017; Mathew et al. 2018). Similarly, the magnitude of the winter freshening in the SEAS varies from year to year (Subrahmanyam et al. 2011; Rao et al. 2015; Mathew et al. 2018). These variations have been attributed to anomalous horizontal advection (Nyadjro et al. 2012), possibly induced by the remote influence of the Indian Ocean Dipole (Subrahmanyam et al. 2011), an indigenous interannual climate mode of the tropical Indian Ocean (Saji et al. 1999). It has further been suggested that this interannual variability in SEAS SSS influences ASWP barrier layer thickness and SST (Sanilkumar et al. 2004). Negative SSS anomalies in the SEAS indeed appear to precede stronger Indian summer monsoon (Neema et al. 2012), suggesting that intensified freshening may enhance vertical stratification and promote further ASWP warming (Nyadjro et al. 2012). In contrast, other authors argue that interannual SST variations in the SEAS are largely attributable to latent and shortwave heat flux variations, rather than to salinity-induced vertical processes (Mathew et al. 2018).

The above literature review reveals that the influence of the winter freshening in the SEAS on the ASWP and monsoon onset is far from a consensus. Indeed, some studies argue that the salinity stratification plays a dominant role on the ASWP at both seasonal (Shenoi et al. 1999, Durand et al. 2004; Hareesh Kumar et al. 2009) and interannual timescales (Neema et al. 2012; Nyadjro et al. 2012) while others argue that its contribution is marginal (Kurian and Vinayachandran, 2007; Mathew et al. 2018). These discrepancies can be attributed in part to the different tools and strategies used to address these issues. For instance, analyses of two ocean general circulation models (Durand et al. 2004; Kurian and Vinayachandran, 2007) yielded very different results regarding the influence of salinity on pre-monsoon heat accumulation in the SEAS, suggesting that results may be model

dependent. Similarly, the nature and role of interannual SSS variations in the SEAS have been inferred from analyses covering a short time period (Subrahmanyam et al. 2011) and/or using salt and heat budgets analyses that are not closed (Nyadjro et al. 2012; Mathew et al. 2018). Finally, most of the studies that have assessed the influence of SEAS salinity stratification on subsequent monsoon onset have relied on statistical analyses rather than detailed process studies. The only study that addresses this issue using sensitivity experiments with a coupled model (Masson et al. 2005) suggests that this salinity stratification enhances the spring warming in the SEAS by 0.5°C and leads to increased rainfall in May related to an early monsoon onset. However, the model used had a relatively coarse horizontal resolution (about 200 km) and had biases such as a too deep mixed layer in the SEAS in winter, which led the authors to recommend the use of higher resolution coupled model to investigate the robustness of their results.

The purpose of this paper is to re-examine the characteristics and drivers of SSS variability in the SEAS, and its influence on the ASWP formation and monsoon onset. To this end, we will use an eddy-permitting ocean model (Akhil et al. 2014, 2016), both forced with an observationally derived dataset and coupled with a regional atmospheric model (Krishnamohan et al. 2019). The paper is organised as follows. Section 2 describes our baseline simulations and sensitivity experiments, the heat and salt budget computation in the mixed layer, and validation datasets. Section 3 evaluates the ability of our simulations to reproduce the salient oceanic features of the SEAS, identifies the processes that drive the seasonal variations in SST and SSS using mixed layer budgets, and finally quantifies the impact of the SEAS salinity stratification on the ASWP formation and monsoon onset through coupled model sensitivity experiments, in which the impact of salinity on vertical mixing is not considered. Section 4 then describes the interannual variability of SSS and SST in the SEAS and their main drivers. The final section summarizes our results and discusses their relevance in light of previously published literature.

2. Data and methods

2.1 Forced model experiments

Here, we use the same regional Indian Ocean configuration as in Akhil et al. (2014, 2016), built from the Nucleus of European Modeling of Ocean (NEMO) ocean general circulation model (Madec, 2008). This configuration covers the entire Indian Ocean (27°E - 142°E , 33°S - 30°N) and uses a $1/4^{\circ}$ horizontal grid and 46 vertical levels, with a vertical resolution increasing from 6 m at the surface to 250 m at the bottom. The reader will refer to Akhil et al. (2014) for a more detailed description of this configuration.

We use the same atmospheric forcing as in Akhil et al. (2015, 2016): air-sea fluxes are

computed using bulk formulae (Fairall et al. 2003) from the model SST and specified atmospheric variables. Most of these near-surface variables (wind, air temperature and specific humidity, downward longwave fluxes) are derived from the Drakkar Forcing Set (DFS) 5.2 forcing product (Dussin et al. 2014), with the exception of downward shortwave radiation, which is based on the TropFlux product (Kumar et al. 2012) and rainfall, which is based on Global Precipitation Climatology Project (GPCP) (Huffman et al. 1997). The simulation also accounts for the interannual variations in runoff from the main rivers flowing into the BoB (Ganges-Brahmaputra, Irrawaddy, Mahanadi, Godavari, Krishna, Cauvery; Akhil et al. 2016). Monthly runoff data is derived from altimeter data for the Ganga-Brahmaputra and Irrawaddy rivers (Papa et al. 2010, 2012). For the rivers along the east coast of India (Mahanadi, Godavari, Krishna & Cauvery) we used the interannual gauge discharge data. It is important to note that we do not apply any relaxation to an observationally derived SSS climatology in any of the simulations.

We use this ocean model configuration and forcing to run a reference experiment (hereafter F-REF) over the period 1990–2012, with lateral boundary conditions based on outputs from a $1/4^\circ$ global ocean run (Brodeau et al. 2010). It is initialized from the World Ocean Atlas temperature and salinity climatologies (Locarnini et al. 2010). The first three years of the simulation are not analysed, in order to allow sufficient time for the upper ocean to adjust: all the analyses are therefore based on the period 1993–2012. These experiments have been used in previous publications, and validations indicate that they reproduce seasonal (Akhil et al. 2014) and interannual variability of SSS in the BoB (Akhil et al. 2016), as well as variability over various other Indian Ocean regions and over a wide range of timescales (Nisha et al. 2013; Vialard et al. 2013; Keerthi et al. 2013, 2016; Kumar et al. 2014).

2.2 Coupled model experiments

To assess the impact of upper ocean salinity stratification on ASWP build-up and monsoon onset, we use the same regional Indian Ocean coupled model setup as in Krishnamohan et al. (2019), which is itself closely related to Samson et al. (2014). Readers can refer to that reference for more details on the coupled model. This model couples a very similar version of the ocean model to the one described in Section 2.1 to the WRF (Weather Research and Forecasting Model) atmospheric model (Skamarock and Klemp, 2008) using a common $1/4^\circ$ horizontal grid for the ocean and atmosphere. The atmospheric component has 28 sigma vertical levels (with a higher resolution of 30 m near the surface). Samson et al. (2014) and Krishnamohan et al. (2019) extensively validated this regional climate model and demonstrated its ability to capture the key features of the Indian Ocean

climate, including the monsoon and variability associated with the Indian Ocean Dipole.

The reference and sensitivity experiments we analyse here are the CTL and NOS experiments from Krishnamohan et al. (2019) (see their table 1 and the accompanying descriptions). The 18-year coupled reference simulation (hereafter, C-REF) is run over the period 1990-2007, with lateral boundary conditions based on ERA-Interim (Dee et al. 2011) for the atmosphere and from a $1/4^\circ$ global ocean run (Brodeau et al. 2010) for the ocean. We also use a sensitivity experiment (hereafter, C-NOS) performed over the same period to test the impact of SEAS haline stratification on the ASWP and summer monsoon onset. This sensitivity experiment is similar to C-REF, except that the Brünt-Vaisala frequency used in the mixing scheme is computed based on a constant salinity value over the region $[5^\circ\text{S}-25^\circ\text{N}; 65^\circ\text{E}-105^\circ\text{E}]$, which includes the BoB and the SEAS. This neglects the effects of the salinity stratification on the vertical mixing in this region. We have not performed a similar “NOS” experiment in the forced model, because the specification of near surface air temperature and humidity in this model amounts to imposing a strong relaxation towards observed SST values, and would not really allow to estimate the effect of the salinity stratification on the SST.

2.3 Validation Datasets

The realism of the modeled SSS seasonal variability is assessed by comparing it to the climatology derived from the European Space Agency (ESA) Climate Change Initiative (CCI) SSS version 3 monthly product, which merges remotely sensed SSS data from the Soil Moisture and Ocean Salinity (SMOS) (Boutin et al. 2018), Aquarius and Soil Moisture Active and Passive (SMAP) satellites (Meissner et al. 2018). This dataset has been shown to capture seasonal and interannual variability in the BoB (Akhil et al. 2020), particularly along the east coast of India, which is an upstream fresh water source for the SEAS. We also used all the available World Ocean Database (WOD, Boyer et al. 2018) in situ SSS measurements between 2002 and 2012 in the SEAS area (outlined on Figure 2). The WOD dataset gathers data from different sources such as CTD (Conductivity Temperature Depth) casts from cruises, Argo (Array for Real time Geostrophic Oceanography), XCTD (eXpendable Conductivity Temperature Depth), gliders, etc.

For SST, we use monthly averages of the 0.25° spatial and 5-day temporal resolution ‘National Oceanic and Atmospheric Administration (NOAA) High-resolution Blended Analysis OI-SST v2’ data for the 1993 to 2012 period. The surface circulation is estimated from monthly averages of the daily 0.25° Geostrophic and Ekman Current Observatory (GEKCO; Sudre et al. 2013) surface current which includes both a geostrophic component computed from satellite altimetry and an Ekman component estimated from scatterometer winds. Sea Level Anomalies (SLA) are taken from the AVISO dataset (Ducet et al. 2000) which merges data from different

altimeters, at 0.25° spatial and monthly temporal resolution. The mixed layer depth (MLD) and barrier layer thickness (BLT) are compared with the gridded in situ 1° monthly climatology of de Boyer Montegut et al. (2004, 2007), which is derived from individual Argo profiles.

Climate indices

To understand the origin of the interannual SSS variability in the SEAS, we relate the year to year salinity fluctuations to the Indian Ocean dipole (IOD; Saji et al. 1999). The most widely used index for IOD is the Dipole mode index (DMI; Saji et al. 1999), defined from the difference between SST anomalies in the western and eastern equatorial Indian Ocean. However, previous studies have indicated that the DMI captures not only the dynamical perturbations associated with the IOD, but also the high-frequency SST perturbations driven by synoptic atmospheric variability (e.g. Dommenget and Jansen, 2009). Akhil et al. (2020) then compared the DMI to several other indices proposed in the literature, and concluded that the most robust IOD index over the recent period was a sea-level based dipole index (SDI) defined as the difference in averaged sea-level anomalies (relative to the mean seasonal cycle) between the southcentral Indian ocean [5°S-15°S; 65°E-90°E] and near Java/Sumatra coast [0°-10°S; 95°E-105°E]. Therefore, we use the SDI as the IOD index in the current study. However, the results are qualitatively similar when obtained using the DMI or any of the other indices discussed in Akhil et al. (2020) (not shown).

2.4 Mixed layer heat and salinity budget

The processes that control the SSS and SST variability in the SEAS are evaluated in the forced and coupled simulations described in section 2.1 and 2.2 using an online heat and salt budget. This online heat and salt budget is vertically integrated over the oceanic mixed layer, as originally described in Vialard and Delecluse (1998). As detailed in Akhil et al. (2014, 2016), the time-varying mixed layer depth used in the entire manuscript is defined as the depth where the potential density increases by 0.01 kg.m⁻³ relative to the surface density. The mixed layer temperature budget is as follows:

$$\partial_t T_{ml} = \underbrace{-\frac{1}{h} \int_{-h}^0 u \partial_x T dz - \frac{1}{h} \int_{-h}^0 v \partial_y T dz}_{\text{horizontal advection}} - \underbrace{\frac{1}{h} \int_{-h}^0 D_l(T)}_{\text{lateral processes}} - \underbrace{\frac{1}{h} (T_{ml} - T_{-h})(w_{-h} + \partial_t h) - \frac{1}{h} [K_z \partial_z T]_{-h}}_{\text{subsurface vertical processes}} + \underbrace{\frac{Q_s(1 - F_{-h}) + Q_{ns}}{\rho_0 C_p h}}_{\text{atmospheric forcing}} \quad \text{--- (1)}$$

In the equation above, T_{ml} is the mixed layer average temperature, a very accurate proxy for

SST, h is the time-varying model mixed layer, (u,v) are the components of the horizontal current, $D_l(T)$ is the model horizontal diffusion operator, w_{-h} is the vertical velocity at the base of the mixed layer, $[K_z \partial_z T]_{-h}$ is the vertical turbulent flux at the base of the mixed layer and K_z the vertical mixing coefficient, Q_s and Q_{ns} are respectively the solar and non-solar components of the surface heat flux, F_{-h} the fraction of the solar radiation at the depth h , ρ_0 the seawater reference density, and C_p the sea water volumic heat capacity. The first term on the right hand side (RHS) represents the effect of horizontal temperature advection in the mixed layer (labelled H.adv in the figures); the second term represents lateral mixing (it will not be discussed in the following as it is always negligible in the present analysis); the third term represents subsurface vertical processes (the combined effect of entrainment, vertical mixing and upwelling; labelled V.proc) and the last term the effect of atmospheric heat fluxes on the mixed layer (labelled SURF).

In a similar way, the mixed layer salinity budget can be written as:

$$\partial_t S_{ml} = \underbrace{-\frac{1}{h} \int_{-h}^0 u \partial_x S dz - \frac{1}{h} \int_{-h}^0 v \partial_y S dz}_{\text{horizontal advection}} - \underbrace{\frac{1}{h} \int_{-h}^0 D_l(S)}_{\text{lateral processes}} - \underbrace{\frac{1}{h} (S_{ml} - S_{-h})(w_{-h} + \partial_t h) - \frac{1}{h} [K_z \partial_z S]_{-h}}_{\text{subsurface vertical processes}} + \underbrace{\frac{1}{h} (E - P - R) S}_{\text{atmospheric forcing}} \quad \text{--- (2)}$$

As for temperature, in equation 2, the first term on the RHS represents the horizontal salinity advection in the mixed layer (H.adv), the second represents the lateral mixing which is neglected in the following, the third represents the subsurface vertical processes (V.proc) while the last term represents the atmospheric forcing (SURF) in which E is the evaporation, P the precipitation, and R the river runoff.

3. SEAS seasonal SSS variability and its impact on SST and rainfall

In this section, we first describe the main features of the SEAS seasonal variations, and evaluate the ability of the forced (F-REF) and coupled (C-REF) reference simulations to simulate these features (Section 3.1). We then evaluate the main mechanisms responsible for the winter freshening and spring warming in the SEAS by analysing the online mixed layer salt and heat budgets in the forced and coupled simulations (Section 3.2). Finally, we quantify the impact of the SEAS haline stratification on the ASWP build-up and monsoon onset by comparing our reference coupled experiment with one in which the influence of salinity on vertical mixing is not considered (Section 3.3).

3.1 Forced and coupled model evaluation

Figure 1 compares the seasonal climatology of key oceanic parameters averaged over the SEAS [70-77°E, 5-12°N] region in the F-REF and C-REF experiments to the observed one. Figure 2 further compares the climatological maps of these parameters in the northern Indian Ocean averaged over December to February (DJF), i.e., when the SEAS is the freshest. The SEAS indeed displays rather salty (above 35ps) waters from June to November in observations followed by a sharp surface freshening in December, then a minimum SSS around 34.5ps in January-February and finally a gradual recovery to summer values (Fig. 1b). Figure 2a further reveals that this winter freshening signal is strongest along the east coast of India and its southern tip and extends into the SEAS and the west coast of India. During that season, the strong seasonal coastal currents are cyclonic, i.e., the EICC in the BoB is southward, the NMC south of India is westward, and the WICC in the SEAS is Northward (Fig. 2b). This is consistent with a prominent role of lateral advection in driving the SEAS freshening (e.g. Durand et al. 2007; Nyadjro et al. 2012). As discussed in the introduction, those currents are associated with a downwelling coastal Kelvin wave at that season, as can be seen from the anomalously high sea level (Fig. 2b, Fig. 1c). Part of that downwelling signal radiates westward as a downwelling Rossby wave (Fig. 2b). As discussed by Durand et al. (2007), the combination of this downwelling signal (Fig. 1c) with an upper ocean freshening due to the freshwater input from the BoB (Fig. 1f, Fig. 2c) leads to a thick barrier layer in the SEAS during winter (Fig. 1e), which extends offshore towards the southern central Arabian Sea (Fig. 2c). This barrier layer reaches a maximum vertical extension around January (~30m) and quickly recedes from March onward (Fig. 1e), under the action of upwelling (marked by a decreasing sea level, Fig. 1c) and increasing SSS (Fig. 1c; see also Durand et al. 2007). The SEAS freshening and thick barrier layer during December-February is followed by a rapid SST warming from February onwards, giving rise to fully developed ASWP in April-May (Fig. 1a).

The forced simulation F-REF displays a ~0.5 salty bias during summer and the coupled simulation a ~0.8 fresh bias during November-December and a ~0.5 fresh bias throughout the rest of the year (Fig. 1b). Despite these biases, both simulations capture reasonably well the SEAS seasonal SSS evolution, with a correct timing for the freshening and salinity minimum (red and green lines on Fig. 1b). The winter SSS pattern in the northern Indian Ocean also compares favourably with observations in both simulations, with freshwaters from the BoB western rim expanding around the southern tip of India into the SEAS (Fig. 2a,d,g). This winter freshening is associated with a sea-level high (deep thermocline) and cyclonic currents in the SEAS (Fig. 1c,d and Fig. 2b,e,h) that compare favourably with observations. We do not show thermocline depth, but its variations largely

mirror those of the sea-level in the SEAS (figure not shown), and we will use sea-level as a proxy for thermocline depth variations in the rest of the paper. F-REF and C-REF MLD seasonal evolution is in phase with the observed climatology, with C-REF MLD ~5-10m shallower than F-REF MLD during June -August and September-November. The coupled model rainfall has a very close seasonal cycle to that of the forced model rainfall (GPCP) over the SEAS (not shown), with monthly errors < 1 mm/day. The thick barrier layer (BLT) that forms in winter in both experiments is also in reasonable agreement with observational estimates (Fig. 1e,f and Fig. 2c,f,i). Despite a cold bias in both F-REF (~ -0.1°C) and C-REF (~ -0.4°C), the seasonal evolution of SST is in phase with the observed climatology, resulting in a fully developed ASWP in April-May as in the observed climatology (Fig. 1a). This is particularly remarkable for the regional coupled model, which has no restoring to the observed SST. This favourable comparison indicates that these forced and coupled simulations are valuable tools to investigate the processes responsible for the SEAS SSS and SST seasonal variations. The coupled model tends to have larger biases (a fresh and cold surface bias), and we will discuss their potential effects on our results in the final section.

3.2 Mechanisms driving SEAS SST and SSS variations

The processes controlling the SEAS SSS and SST seasonal evolution in these simulations are further detailed based on the online mixed layer salt and heat budgets described in Section 2.5 (Fig. 3). Both simulations experience a large SSS drop in the SEAS in November and December (Fig. 3a). Comparison of Figure 3b and 3c indicates that the processes controlling the seasonal salinity evolution are very similar in both simulations. The total tendency term (black curves) is to a large extent driven by horizontal advection (blue curves). This advection-induced winter freshening is largest in December (Fig. 1b,c), when the poleward currents are strongest (Fig. 1d): this confirms the role of the WICC for advecting freshwater originating from the BoB into the SEAS. Salinity increases with depth throughout the year in the SEAS, resulting in a subsurface process that always tends to increase the SSS. In winter, however, the freshening of the surface increases the salinity stratification so that the saltening effect of subsurface processes increases. As a result, vertical processes tend to dampen the freshening induced by horizontal advection during winter (red curves on Fig. 3b,c). Finally, surface forcing has a second-order effect (green curves on Fig. 3bc), freshening the surface layers during and just after the monsoon through rainfall, and saltening the surface layers in winter and spring when surface evaporation dominates. Overall, the dominant balance that explains the SEAS SSS freshening in both models is the advection of freshwater from the BoB in winter, with the downward mixing of freshwater acting as a restoring force to climatology.

As for SSS, the SEAS SST shows a very similar seasonal evolution in F-REF and C-REF (Fig. 3d), with a strong SST increase from $\sim 28^{\circ}\text{C}$ in February to $\sim 30^{\circ}\text{C}$ in April. The processes controlling this seasonal SST evolution are also qualitatively similar between these two simulations (Fig. 3e,f): the intense spring warming (black curves) is indeed mainly due to net surface heat fluxes into the ocean (green curves) during this season, when the sun is at zenith and monsoon clouds have not yet formed. This warming by surface heat fluxes is partly offset by a cooling through vertical processes (red curves). The decrease in SST after May tends to be driven by subsurface processes with a non-negligible contribution from evaporative/shortwave cooling (Fig. 3e,f), induced by the summer monsoonal wind forcing. In contrast with SSS seasonal variations, horizontal advection plays a minor role in driving seasonal SST variations in the SEAS (blue curves on Fig. 3e,f). The shape of the seasonal SST evolution is thus largely determined by the balance between net surface heat fluxes and vertical oceanic processes. In F-REF and C-REF, however, wintertime is a very special period, when vertical processes do not cool but rather warm the SEAS ocean surface, by $\sim 0.3\text{-}0.4^{\circ}\text{C}\cdot\text{month}^{-1}$ in December and January (Fig. 3e,f). Previous studies (Durand et al. 2004; Hareesh Kumar et al. 2009; Masson et al. 2005, Nyadjro et al. 2012) suggest that this warming tendency is clearly attributable to temperature inversions, associated with the strong barrier layer that occurs during this season (Fig. 1e). However, this warming is offset by a cooling induced by net heat flux forcing during that season as well as by horizontal advective processes. The impact of this salinity-induced warming on the warm waters build-up in the subsequent months is quantified in the next subsection using sensitivity experiments with the regional coupled model.

3.3 Influence of SEAS seasonal SSS variations on the monsoon

The analyses performed in the previous subsections indicate that the C-REF experiment captures the salient features of the salinity and barrier layer seasonal evolution in the SEAS. Furthermore, the processes responsible for the SEAS SSS and SST evolution (and in particular the occurrence of warming by subsurface processes) are robust in the two simulations. This robust representation of salinity-related processes in C-REF gives us confidence in using this coupled model to diagnose the effect of the SEAS salinity on the ASWP and monsoon. To this end, we compare our coupled reference experiment (C-REF) with the sensitivity experiment where we neglect the influence of salinity stratification on vertical mixing, which also as a consequence would remove the formation of barrier layer (C-NOS, see section 2.2 and Krishna Mohan et al. (2019) for a detailed description of this experiment).

Figure 4a,b compares the SST and rainfall climatology in the two simulations. One would expect a cooler SST in the C-NOS after December-February, which is after the season when salinity

stratification is the strongest and barrier layers are thickest as salinity stratification will indeed limit the cooling by vertical processes and barrier layer store heat in the subsurface. Fig. 4a however indicates that this is not the case, with almost no differences between the C-REF and C-NOS SST at the end of February (and in fact a slightly warmer SST in C-NOS). As a result, rainfall changes are very small both locally over the SEAS (Fig. 4b) and over the Indian subcontinent (not shown).

The mixed layer heat budget analysis on Figure 3f indicates a warming through vertical processes of about 0.3°C in December and 0.5°C in January. Such a warming can only occur in presence of salinity stratification, and thus salinity contributes to warm the mixed layer by at least 0.8°C during December-January. Figure 4c provides insights into why this impact of salinity on vertical processes does not influence SST, by displaying the C-REF minus C-NOS mixed layer heat budget terms, i.e., the salinity stratification impact on the SST budget. This analysis quantifies the overall effect of the salinity stratification, which is not limited to the entrainment warming described above, as salinity also contributes to diminish entrainment cooling. Overall, salinity stratification contributes to intensifying the warming (or reducing the cooling) of the mixed layer through vertical processes by $0.6\text{-}0.9^{\circ}\text{C}\cdot\text{month}^{-1}$ during December-February and $0.2^{\circ}\text{C}\cdot\text{month}^{-1}$ during March. This should result in a 3°C warming of the SEAS SST over this period.

However, this warming tendency due to subsurface processes is offset by a cooling tendency due to atmospheric forcing, resulting in very small differences in the total SST tendency term (Fig. 4c) and thus a similar SST seasonal evolution in the C-REF and C-NOS experiments (Fig. 4a). Additional analyses reveal that the net surface heat flux into the ocean is nearly identical between the two experiments (not shown). The anomalous atmospheric cooling that counteracts the warming by vertical processes is instead the result of changes in the mixed layer depth, which is ~ 15 m deeper in C-NOS from December to February (Fig. 4d). This can be explained as follows. Climatological net surface heat fluxes are negative (the ocean loses heat) in the SEAS from December to February, i.e. in boreal winter. Salinity stratification results in a shallower MLD during this season, which cools more under the influence of the upward net surface heat flux due to its reduced heat capacity. In addition, this MLD shoaling results in an increase in the amount of solar radiation penetrating below the base of the mixed layer, which contributes to enhance the atmospheric cooling tendency. Overall, therefore, there is an offset between the salinity-induced warming by vertical processes and salinity-induced cooling in relation to a thinner mixed layer, resulting in almost no salinity-induced change in SST in the SEAS region, and thus no change in rainfall locally or over India.

4. SEAS interannual SSS variability

The previous section identified the dominant processes responsible for the SST and SSS seasonal variations in the SEAS from the combined analysis of experiments performed with a forced

and coupled model. In this section, we seek to understand the main drivers of interannual variability in the SEAS. Unfortunately, the interannual SSS variability in the coupled model is about five times weaker than in the forced model (not shown) and in observational estimates discussed below. This section will therefore focus on the analysis of the forced model experiment. We will first describe the modelled interannual signals in the SEAS region and qualitatively compare them with observations (section 4.1) before discussing their driving mechanisms (section 4.2).

4.1 Modelled interannual variability in the SEAS region

Figure 5 provides an overview of the regions with the highest interannual SSS variability (hereafter, SSS' refers to SSS anomalies relative to the climatological seasonal cycle) as a function of season in F-REF experiment and in observations (CCI-SSS). The BoB shows the greatest SSS' variability in fall, with maximum signals located around its western rim (Fig. 5a). These signals have been discussed in Akhil et al. (2016), Fournier et al. (2017) and Akhil et al. (2020) and attributed to the remote influence of equatorial wind signals associated with the IOD. The F-REF SEAS SSS' variability is small during SON (Fig. 5a) but increases dramatically in DJF (Fig. 5b), reaching up to 1psv near the coast. This area of maximum variability shifts northwestward during the following spring (Fig. 5c) and disappears in summer (not shown). Although the observational standard deviation is obtained over a different period (1993 to 2012 for F-REF vs 2010 to 2019 for the CCI-SSS), it allows a qualitative comparison. The patterns and seasonal evolution of the SSS interannual variability amplitude agree qualitatively, but the model clearly overestimates the SSS variability in the SEAS region (almost by a factor 2). We will come back to the potential consequences of this overestimation on our results in the discussion section.

The model SEAS SSS' is shown in Figure 6a, with SSS anomalies up to 1psv during the winter that follow IOD events (red and blue vertical bars in Fig. 6a, saltening after positive IOD events and freshening after negative ones). Unfortunately, there are not enough SSS observations in in situ databases such as the World Ocean Dataset (Locarnini et al. 2010) to provide a quantitative comparison. Instead, we will show a comparison of SSS anomalies maps of remotely sensed data after the 2010 negative and 2011 positive IOD events, years for which both the model and satellite data are available. Reassuringly, however, the model accurately captures SST' (Fig. 6b) and SLA' (Fig. 6c), with correlations to observations of ~ 0.8 . Overall, IOD events are tightly related to the interannual fluctuations in boreal fall in the SEAS: positive IOD events are generally associated with a positive SSTA and SLA in SON, and a positive SSS anomaly in DJF, with opposite signals during negative IOD events.

We further characterize the F-REF SEAS interannual variations associated with the IOD variability by performing lead/lag-regression of SSS', SST' and upper ocean stratification indices on the normalized SDI index in SON (Fig. 6d-f). This analysis first indicates that typical SST' and SLA' show a very similar evolution in the model and observations during an IOD. Warm anomalies develop in the SEAS during the boreal summer and fall, before and during the peak of a positive IOD event; and decrease the following months (Fig. 6e). Positive SSS anomalies appear shortly after the IOD peak, are maximum in December-January and slowly decrease thereafter (Fig. 6d). This IOD-induced anomalous saltening in winter (Fig. 6d) is associated with an anomalously deep MLD (up to ~3m) in the early boreal winter. This is likely in response to weaker-than-usual haline stratification, since there are no significant changes to local wind and surface buoyancy fluxes over the SEAS in winter during IOD events (Fig. 11cg of Keerthi et al. 2013). As shown on Figure 6f, SLA' changes sign during an IOD: positive IOD events are first associated with a SLA increase in the SEAS from summer to fall, followed by a rapid SLA decrease that leads to marginally significant negative SLA anomalies during the following winter. The anomalous thermocline shoaling implied by these negative SLA anomalies (Fig. 6f) combines with the deeper-than-usual MLD to reduce the BLT by as much as 4m at the end of the winter season (Fig. 6f).

Although we do not have a sufficiently long SSS time series to statistically estimate the observed IOD-induced variations in the SEAS, we qualitatively compare the CCI and F-REF SSS anomalies after events during the common record: after the negative 2010 and positive 2011 IOD events (Fig. 7.). Overall, there is a good qualitative agreement between F-REF and remotely-sensed observations, with a freshening (saltening) around the southern tip of Indian and in the SEAS after the 2010 negative (2011 positive) IOD event. However, the remotely sensed signal is weaker than the model signal, in particular in 2011 IOD event. We will come back to this point at the end of section 4.2.

Overall, the model indicates an anomalously salty and warm SEAS with deeper-than-usual MLD in the SEAS during the winter after positive IOD events (and opposite signals for negative events). We do not have sufficient SSS data to confirm the modelled SSS salinity signals, but the good representation of interannual SST and sea level variability in the SEAS and qualitatively correct (but overestimated) SSS signals after two IOD events are reassuring about the model's ability to reproduce interannual SEAS variations.

4.2 Mechanisms driving SEAS SST and SSS interannual variations

Typical interannual signals associated with the IOD are mapped on Figure 8, through a lag-regression of SON and DJF oceanic fields on the normalized SON SDI index. As already detailed in Akhil et al. (2016), Figure 8a indicates that IOD events are typically associated with positive SSS anomalies along the east coast of India, and an anomalous freshening in the Andaman Sea and eastern equatorial Indian Ocean. It is also showed by the two observed cases on Fig. 7. Akhil et al. (2016) demonstrated that easterly wind signals during positive IOD events induce upwelling coastal Kelvin waves that propagate counter-clockwise along the BoB rim (Fig. 8b). These waves induce anti-cyclonic anomalous currents (Fig. 8b) on top of the climatological cyclonic circulation (Fig. 8a), and thus reduce the southward transport of freshwater from the Northern BoB by the EICC (Fig. 8b). In agreement with Figure 6a,d, the SEAS does not show significant salinity signals during the IOD mature phase (Fig. 8a) but experiences positive sea-level anomalies extending over the entire southern Arabian Sea (Fig. 8b). Along the west coast of India, this sea level rise has been attributed to IOD-induced easterly wind anomalies near the southern tip of India (Suresh et al. 2018), which drive shoreward Ekman transport and generate a downwelling coastal Kelvin wave.

During winter, the salty anomaly decreases along the east coast of India but expands in the SEAS region and along the west coast of India (Fig. 8d). The correlation between SON SSS' and SDI is greater than 0.8 both in the western BoB in fall (contours on Fig. 8a) and in the SEAS in winter (contours on Fig. 8d), illustrating the tight control of SSS anomalies in F-REF by the IOD in these two regions. The sign reversal of the sea-level signal along the west coast of India from positive in fall to negative in winter seen on Figure 6f is also evident on Figure 8b,e. These negative winter sea-level anomalies following positive IOD events have been linked to the delayed remote effect of fall equatorial easterlies (Suresh et al. 2018). These wind anomalies force upwelling Kelvin waves that reflect off the eastern boundary as equatorial upwelling Rossby waves, eventually reaching the southern tip and propagating to the west coast of India and SEAS in winter (Fig. 8e; Suresh et al. 2018).

Now that we have described the basin-scale signals associated with IOD events, we will further detail the causes of the SST and SSS anomalies in the SEAS by analysing the online mixed layer salt and heat budget in the F-REF experiment (Fig. 9). The mechanisms driving the SEAS SSS' response to the IOD have some similarities to the ones described at the seasonal timescale (section 3.2 and Fig. 3b). The development of the salty signal in November (Fig. 9a) is largely the result of anomalous horizontal advection (Fig. 9b). As shown in Figure 8d, strong seasonal alongshore

currents at the southern tip and along the west coast of India indeed advect the SON salty anomalies (Fig. 8a) along the east coast of India to the west coast during a positive IOD event, resulting in a SEAS salty anomaly that peaks in December (Fig. 9a,b). As soon as the surface salinity increases and reduces the salinity vertical gradient and upward mixing of salt, the vertical processes anomalies become negative and dampen the effect of horizontal advection in December and overcome it from January onward, slowly restoring salinity to its climatological value after the end of boreal winter (Fig. 9b). Overall, the winter SSS anomalies in the SEAS are thus resulting from the advection of the western BoB signals from the previous fall, and then dissipated by vertical oceanic processes.

While IOD-related SSS' signals appear only in winter in the SEAS, SST' signals appear earlier (Fig. 9a,c). The southern AS warming is already evident in summer, peaks in fall and then slowly decays afterwards (Fig. 9c), with a maximum warming located along the southwest coast of India in fall (Fig. 8c). As shown on Figure 9d, the horizontal advection of heat is generally negligible, and the atmospheric forcing term is not responsible for this warming and instead acts as a negative damping (Fig. 9d), probably because positive SST anomalies tend to be associated with enhanced rainfall and cloudiness over the Indian Ocean (Izumo et al. 2020). Instead, the SEAS warming in summer and early fall is due to a reduction of the cooling by vertical mixing until November. There are no barrier layer anomalies until December (Fig. 1e), and no SSS anomaly. The vertical salinity stratification below the MLD also does not change in the early phases of the warming (not shown), and hence cannot explain it. There are on the other hand significant positive sea level anomalies since July, indicating a deeper than usual thermocline. The resulting weaker temperature gradient below the mixed layer results in a weaker cooling through vertical processes, i.e. a surface warming. This analysis is consistent with the results of Murtugudde et al. (2000) who attributed the IOD-induced warming signal in the northwestern Indian Ocean to the effect of anomalous downwelling signal induced by a thermocline deepening that prevents entrainment cooling. The vertical processes then change sign, and contribute to an anomalous cooling of the mixed layer by up to $0.2^{\circ}\text{C}\cdot\text{month}^{-1}$ during December-February (Fig. 9d), which contributes to the slow decline of warm anomalies in the SEAS region (Fig. 9c). This can be attributed to the development of negative sea level anomalies at that time (Fig. 6f, 8e) which induce an anomalously shallow thermocline, as well as an anomalously thin barrier layer (Fig. 6f) and weakened salinity stratification below the mixed layer (not shown) which may also contribute to the enhanced cooling. Overall, the main driver of the development of positive SST anomalies in the SEAS region during August-October of a positive IOD event is therefore reduced cooling by subsurface processes in relation with the anomalously deep thermocline. The warm anomaly then drives enhanced heat losses

to the atmosphere, which then slowly restore the SST to its climatological value.

Most of the IOD-related haline stratification changes in the SEAS occur in winter, while the SST anomalies are already declining. The weaker salinity stratification associated with the SSS increase and thin SEAS BLT during the winter following positive IOD events (Fig. 6f) may contribute to the enhanced cooling tendency by vertical processes (Fig. 9d). However, the relative effect of this haline stratification change and of the thermocline is not easily quantified. Furthermore, most of this anomalous cooling is offset by an anomalous warming due to atmospheric forcing, resulting in a weak (up to $-0.1^{\circ}\text{C}\cdot\text{month}^{-1}$) and barely significant SST change in that season (Fig. 9e). The inability of the coupled experiment to accurately simulate the SEAS interannual variability does not allow us to properly quantify the specific influence of SSS' variations on the mixed layer heat budget. However, we can expect this effect to be small. Indeed, completely neglecting the salinity stratification at the seasonal timescale in the C-NOS experiment resulted in almost no changes in the SST, so one may expect smaller salinity stratification changes associated with the IOD to play an even smaller role. Finally, the limited observational comparison dataset that we have suggests the model may overestimate the magnitude of IOD-related SSS anomalies (Fig. 7), further reducing their potential influence on SST. Overall, our results suggest that the influence of interannual SSS anomalies on the interannual SST anomalies in the SEAS is probably quite small, and would only affect the decay phase of the winter SST anomalies.

5. Summary and discussion

5.1 Summary

The SEAS hosts the warmest SST of the world ocean in April-May. This hotspot is thought to play a key role in triggering the Indian summer monsoon. This warm water build-up in the SEAS is preceded by an inflow of freshwater in winter originating from the BoB western rim. Some studies (e.g. Durand et al. 2004; Nyadjro et al. 2012) have proposed that this winter freshening contributes to the warm water buildup in the following months via increased upper ocean stratification that limits cooling by vertical mixing, while others argue for a marginal contribution (Kurian and Vinayachandran, 2007; Mathew et al. 2018). The present study thus aims to revise the understanding of the influence of salinity on the SEAS warm-pool build-up and on the monsoon onset. To that end, we use an eddy-permitting ocean model either in forced mode or coupled to a regional atmospheric model.

Both simulations reproduce the main seasonal hydrographic features of the SEAS reasonably well, including the magnitude and timing of the winter freshening, the associated thick barrier layer

and thin mixed layer, and the seasonal warm water build up. The online mixed layer salinity and heat budgets are in agreement in both the forced and coupled model versions. They confirm the dominant role of freshwater advection from the BoB in the seasonal winter freshening in the SEAS, while vertical processes then act to erode this seasonal freshening. The seasonal heat budget in the mixed layer in these two simulations also reveals that this freshening contributes to the warming of the SEAS by stabilizing the upper ocean and allowing the formation of a thick barrier layer and temperature inversion, resulting in an unusual situation where vertical processes tend to warm the upper ocean in winter. A sensitivity experiment in the coupled model in which the effect of salinity on vertical mixing is turned off allows us to investigate the effect of the seasonal freshening of the SEAS on the SST and the onset of the monsoon. The seasonal mixed layer heat budget indicates that salinity contributes to an enhanced 3°C warming of the SEAS through vertical processes in the months prior the development of the Arabian Sea warm pool. However, this does not lead to a significant SEAS warming at the time of the monsoon onset, as the cooling tendency by atmospheric forcing offsets the salinity-induced warming by vertical processes. Stable salinity stratification indeed yields a shallower winter mixed layer, which is more efficiently cooled by negative surface fluxes due to the combined effects of its reduced heat capacity and enhanced fraction of the surface shortwave flux that escapes through the base of the mixed layer. The very modest SST response to salinity stratification results in an insignificant rainfall response, both locally and over the Indian subcontinent.

In addition to seasonal variations, we also analyse the dominant factors controlling the interannual variability of the SEAS. This analysis is performed only with the forced ocean model, given the inability of the coupled configuration to realistically simulate these interannual variations. The largest interannual SSS anomalies in the SEAS occur in winter, and are strongly associated ($r \sim 0.8$) with the remote influence of the IOD. Akhil et al. (2016) previously showed that the equatorial wind forcing associated with positive (negative) IOD events result in positive (negative) SSS anomalies in the western BoB in September-November, in response to circulation changes transmitted by planetary waves transiting through the equatorial and coastal waveguides. Here we show that the mean circulation associated with the southward EICC, westward NMC south of Sri Lanka, and northward WICC transport these SSS anomalies to the SEAS in December-February, where they are then dissipated through anomalous vertical oceanic processes, which act as a restoring force to subsurface higher-salinity values. SST anomalies begin to develop in the summer before the IOD peak in the SEAS, and thus precede the development of those winter SSS anomalies. Warm SST anomalies develop during positive IOD events in response to the anomalously deep thermocline. It is possible that the reduced salinity stratification through its impact on vertical mixing

and anomalously thin BLT that follow a positive IOD contribute to the decay of the SST anomaly during winter, but this effect is probably small.

5.2 Comparison with previous studies

The dominant role of horizontal advection in SSS variations in the SEAS on both seasonal and interannual timescales highlighted in this study is consistent with previous research on this topic. At seasonal timescales, the SEAS freshening has indeed been consistently attributed to horizontal advection of freshwater from the BoB in both observations (e.g., Rao and Sivakumar, 1999, 2003; Prasanna Kumar et al. 2004) and models (e.g., Durand et al. 2007; Kurian and Vinayachandran, 2007; Nyadjro et al. 2012). Our results confirm these previous findings, but the mixed layer salt budget has additionally allowed us to identify the key role of vertical processes in limiting the magnitude of the freshening and its erosion after winter. While many studies have discussed the mechanisms of seasonal SSS variations in the SEAS, we are aware of only one study that addresses interannual SSS variations (Subrahmanyam et al. 2011). By comparing the SSS in 2005 (a strong negative IOD) and in 2006 (a strong positive IOD) in a gridded Argo product and in an ocean model, these authors hypothesized that the larger SEAS freshening in late 2006 than in late 2005 could be attributed to the IOD. Our modelling results, based on a longer period (~20 years), confirm the dominant role of the IOD in modulating the interannual SSS variability in the SEAS in winter ($r \sim 0.8$). Our mixed layer salinity budget also identifies anomalous horizontal advection as the key process driving this variability. While it is well known that the IOD is a dominant driver of interannual SSS variability in the Equatorial Indian Ocean (e.g., Grunseich et al. 2011; Durand et al. 2013; Nyadjro and Subrahmanyam, 2014; Du and Zhang, 2015) and in the BoB (e.g. Chaitanya et al. 2014; Pant et al. 2015; Akhil et al. 2016; Fournier et al. 2017), the present study further demonstrates its dominant role in controlling the SSS interannual variability in the SEAS.

The influence of this winter SEAS freshening on the mixed layer heat budget is more controversial. Analyses based on two forced ocean general circulation models have shown either a significant (Durand et al. 2004) or marginal (Kurian and Vinayachandran, 2007) influence. Indeed, Durand et al. (2004) found that the cooling effect associated with vertical processes is largely suppressed or strongly reduced from November to May when a thick barrier layer is present, and that vertical processes even warm the mixed layer in December and January ($+0.4^{\circ}\text{C}\cdot\text{month}^{-1}$) when strong thermal inversions occur. The heat budget analyses in our forced and coupled model experiments (Fig. 3) agree very well with those of Durand et al. (2004) (see their Figure 3b), confirming their quantitative estimate of the vertical processes contribution to the mixed layer heat

budget. Our coupled sensitivity experiment also allowed to quantify the magnitude of the salinity-induced warming through vertical processes: $\sim 3^{\circ}\text{C}$ from November to May. In a subsequent modelling study, Kurian and Vinayachandran (2007) conducted sensitivity experiments with a similar model in which salinity was held constant throughout the model domain. Their results indicate that neglecting the effect of salinity did not affect the timing and magnitude of the warm water build-up, in agreement with our sensitivity experiment in the regional coupled model. Kurian and Vinayachandran (2007) however argue that the SEAS SST evolution is dominated by atmospheric forcing in winter and spring and that the formation and maintenance of the ASWP therefore does not depend on near surface stratification. Our explanation is different: we find a stronger salinity-induced warming by vertical processes as in Durand et al. (2004), but a salinity-induced compensating due to the concentration of the winter surface heat losses by atmospheric fluxes over a thinner mixed layer. But in essence our study and that of Kurian and Vinayachandran (2007) are consistent in suggesting a rather weak influence of the SEAS salinity on the ASWP build-up.

Other studies have investigated the SEAS interannual SSS variability. We attribute SSS anomalies in the SEAS to zonal advection, as Nyadjro et al. (2012) and confirm the Subrahmanyam et al. (2011) hypothesis that those anomalies are caused by the Indian Ocean Dipole. It has been further suggested that fresh SSS anomalies in the SEAS tend to induce warmer SST (Sanilkumar et al. 2004), due to reduced cooling through vertical processes (Nyadjro et al. 2012) and to precede stronger than usual Indian summer monsoon (Neema et al. 2012). Mathew et al. (2018) rather concludes that interannual SST variations in the SEAS are largely attributable to latent and shortwave heat flux variations. In our model, the SSS signals appear after the bulk of the SST warming in the SEAS, that we largely attribute to vertical oceanic processes. We find a possible contribution of changes in SSS stratification during the decay of the SST anomaly, but not during its development. As shown by figure 5, our model overestimates SSS interannual variability in the SEAS, so the effect of SSS variations may be even smaller in nature. The poor level of agreement between previous studies however suggests that new modelling and observational studies are needed to conclude about a possible effect of salinity stratification on the SST and atmosphere in the SEAS.

All the studies discussed in the previous paragraphs were conducted using forced ocean model experiments. The only study that could thoroughly evaluate the role of SEAS freshening on regional climate is Masson et al. (2005). Using sensitivity experiments in a global coupled model, they suggest that the salinity stratification in the SEAS results in a 0.5°C warmer spring SST in the

SEAS, and leads to a 15-day earlier onset of the summer monsoon. These results are inconsistent with our set of coupled experiments, which indicates a negligible role of the SEAS freshening on the ASWP build-up and subsequent monsoon onset. This discordance is likely related to the different model configurations used between these two studies. Unlike the present study, which uses a relatively fine horizontal model resolution ($1/4^\circ$), Masson et al. (2005) indeed use a rather coarse horizontal ocean model resolution (2°) and pointed out non-negligible model biases, including a too deep mixed layer in winter, which may alter the reliability of their results. Despite its fairly reasonable representation of the SEAS and enhanced spatial resolution, our model also suffers from biases such as a too cold and fresh surface layer, and a too shallow MLD in summer and fall. Given the antagonistic effect of salinity on the surface layer heat budget, it is difficult to conclude on how these two effects may influence our results. The fresh surface layer and enhanced salinity stratification indeed should reduce cooling by vertical processes. But the resulting shallow mixed layer bias on the other hand enhances the cooling by the winter negative surface heat flux. Further studies with other coupled models which simulates a more realistic mean state and interannual SSS variability will thus be needed to assess the robustness of the influence of the SEAS salinity stratification on the formation of the ASWP and monsoon onset.

Acknowledgments:

The authors are grateful to the Director of CSIR-NIO (“CSIR- National Institute of Oceanography, India”) for providing the facilities and encouragement for the completion of this work. We also thank Institut de Recherche pour le Développement (“IRD”, France) for the support to the collaboration on Indian Ocean research with the CSIR-NIO This is NIO contribution number XXXX.

Declarations :

Ethics approval and consent to participate: Not Applicable

Consent for publication: All authors consent to the publication of the manuscript in Climate Dynamics, up on completion of the peer review.

Availability of data and material: The observed SSS data used in this study is from ESA-CCI+SSS V3 monthly product (<https://climate.esa.int/fr/odp/#/project/sea-surface-salinity>). SST data is from OI-SST V2 (<https://www.esrl.noaa.gov/psd/data/gridded/data.noaa.oisst.v2.highres>). SLA data is from AVISO dataset (www.aviso.oceanobs.com/fr/accueil/index.html). Mixed layer and Barrier layer data is from Ifremer (<https://cerweb.ifremer.fr/deboyer/mld/home.php>).

Competing interests: The authors declare no competing interests.

Funding : The authors acknowledge the support from EEQ/2021/001123 project funded by DST-SERB, CCI+ Sea Surface Salinity project funded by ESA (European Space Agency) and by the SMOS CNES project funding. Keerthi MG is supported through a postdoctoral fellowship from CNES & CNRS, France.

Authors' contribution: VPA, ML, MGK and JV conceived and developed the study. VPA and KSK performed the data analysis and made the plots. VPA, ML and JV made the interpretation of the results and wrote the manuscript. ML and JV supervised the whole research.

Reference

- Akhil, V.P., Durand, F., Lengaigne, M., Vialard, J., Keerthi, M.G., Gopalakrishna, V.V., Deltel, C., Papa, F., de Boyer Montégut, C. (2014). A modeling study of the processes of surface salinity seasonal cycle in the Bay of Bengal. *J. Geophys. Res. Oceans* 119, 3926-3947. doi:10.1002/2013JC009632.
- Akhil, V.P. (2015). Remote sensing and numerical modeling of the oceanic mixed layer salinity in the Bay of Bengal, 192 pages, PhD Thesis, <http://thesesups.ups-tlse.fr/3096/>
- Akhil, V.P., Lengaigne, M., Vialard, J., Durand, F., Keerthi, M.G., Chaitanya, A.V.S., Papa, F., Gopalakrishna, V.V., de Boyer Montégut, C. (2016). A modeling study of processes controlling the Bay of Bengal Sea surface salinity interannual variability. *J. Geophys. Res. Oceans* 121 (12), 8471–8495.
- Akhil, V.P., Vialard J., Lengaigne M., Keerthi, M.G., Boutin, J., Vergely, J.L., and Papa, F. (2020). Bay of Bengal Sea surface salinity variability using a decade of improved SMOS re-processing. *Remote Sensing Environ.*, 248, <https://doi.org/10.1016/j.rse.2020.111964>.
- Brodeau, L., Barnier, B., Treguier, A.M., Penduff, T., Gulev, S. (2010). An ERA40-based atmospheric forcing for global ocean circulation models. *Ocean. Model.* 31(3-4), 88-104. doi:10.1016/j.ocemod.2009.10.005.
- Boutin, J., Vergely, J.-L., Khvorostyanov, D. (2018). SMOS SSS L3 maps generated by CATDS CEC LOCEAN. debias V3.0. SEANOE. <https://doi.org/10.17882/52804#57467>.
- Boyer, T., Locarnini, R. A., Baranova, O., Garcia, H. E., Mishonov, A. V., Paver, C., ... & Zweng, M. (2018). The World Ocean Atlas 2018: improvements and uses of climatological mean fields. In *AGU Fall Meeting Abstracts* (Vol. 2018, pp. OS13D-1506).
- Chacko, K. V., Hareesh Kumar, P. V., Ramesh Kumar, M. R., Mathew, B., & Bannur, V. M. (2012). A note on Arabian Sea Warm Pool and its possible relation with monsoon onset over Kerala. *Journal of Scientific and Research Publications*, 2(12), 286–289.
- Chaitanya, A. V. S., F. Durand, S. Mathew, V. V. Gopalakrishna, F. Papa, M. Lengaigne, J. Vialard, C. Krantikumar, and Venkatesan R. (2014), Observed year-to-year sea surface salinity variability in the Bay of Bengal during the period 2009-2014, *Ocean Dyn.*, doi:10.1007/s10236-014-0802-x.

- Chaitanya, A. V. S., Vialard, J., Lengaigne, M., d'Ovidio, F., Riotte, J., Papa, F., & James, R. A. (2021). Redistribution of riverine and rainfall freshwater by the Bay of Bengal circulation. *Ocean Dynamics*, 71(11), 1113-1139.
- de Boyer Montégut, C., Madec G, Fischer AS, Lazar A, Iudicone D. (2004). Mixed layer depth over the global ocean: an examination of profile data and a profile-based climatology. *J Geophys Res* 109:C12003. doi:10.1029/2004JC002378
- de Boyer Montégut, C., Mignot, J., Lazar, A., Cravatte, S. (2007). Control of salinity on the mixed layer depth in the world ocean: 1. General description. *J. Geophys. Res. Oceans* 112, C6.
- Dee, D. P., et al. (2011). The ERA-interim reanalysis: Configuration and performance of the data assimilation system, *Q. J. R. Meteorol. Soc.*, 137, 553–597, doi:10.1002/qj.828.
- Deepa, R., Seetaramayya, P., Nagar, S.G., Gnanaseelan, C. (2007). On the plausible reasons for the formation of onset vortex in the presence of Arabian Sea mini warm pool. *Curr Sci.* 92:794–800.
- Dommenget, D., & Jansen, M. (2009). Predictions of Indian Ocean SST indices with a simple statistical model: A null hypothesis. *Journal of climate*, 22(18), 4930-4938.
- Du, Y., Zhang, Y. (2015). Satellite and Argo observed surface salinity variations in the tropical Indian Ocean and their association with the Indian Ocean dipole mode. *J Clim* 28:695–713.
- Ducet, N., Le Traon, P.Y., Reverdin, G. (2000). Global high-resolution mapping of ocean circulation from TOPEX/POSEIDON and ERS-1 and -2. *J. Geophys. Res.: Oceans* 105 (C8), 19,477–19,498.
- Durand, F., S. R. Shetye., J. Vialard., D. Shankar., S. S. C. Shenoi., C. Ethe., G. Madec. (2004). Impact of temperature inversions on SST evolution in the South-Eastern Arabian Sea during the pre-summer monsoon season, *Geophys. Res. Lett.*, 31, L01305, doi:10.1029/2003GL018906.
- Durand, F., D. Shankar., C. de Boyer Montégut., S. S. C. Shenoi., B. Blanke., and G. Madec. (2007). Modeling the barrier-layer formation in the Southeastern Arabian Sea, *J. Clim.*, 20, 2109–2120, doi:10.1175/JCLI4112.1.
- Durand, F., G. Alory., R. Dussin., N. Reul. (2013). SMOS reveals the signature of Indian Ocean Dipole events, *Ocean Dyn.*, 63(11–12), 1203– 1212.
- Dussin, R., B. Barnier., L. Brodeau. (2014). Atmospheric forcing data sets to drive eddy-resolving global ocean general circulation models, Abstract 1716 presented at EGU General Assembly Conference Abstracts, vol. 16, p.1716, EGU, Vienna, Austria.
- Fairall, C. W., Bradley, E. F., Hare, J. E., Grachev, A. A., & Edson, J. B. (2003). Bulk parameterization of air–sea fluxes: Updates and verification for the COARE algorithm. *Journal of climate*, 16(4), 571-591.
- Fournier, S.J., Vialard, J., Lengaigne, M., Lee, T., Gierach, M.M., Chaitanya, A.V.S. (2017). Unprecedented satellite synoptic views of the Bay of Bengal “river in the sea”. *J. Geophys. Res. Ocean*, online first, doi: 10.1002/2017JC013333.

- Gadgil, S., P. V. Joseph., N. V. Joshi. (1984). Ocean–atmosphere coupling over monsoon regions, *Nature*, 312, 141–143.
- Gopalakrishna, V. V., Z. Johnson., G. Salgaonkar., K. Nisha., C. K. Rajan., R. R. Rao. (2005). Observed variability of sea surface salinity and thermal inversions in the Lakshadweep Sea during contrast monsoons. *Geophys. Res. Lett.*, **32**, L18605, doi:10.1029/2005GL023280.
- Grunseich, G., B. Subrahmanyam., V. S. N. Murty., B. S. Giese. (2011). Sea surface salinity variability during the Indian Ocean Dipole and ENSO events in the tropical Indian Ocean, *J. Geophys. Res.*, 116, C11013, doi:10.1029/2011JC007456.
- Hareesh Kumar, P.V., Madhu, J., Sanilkumar, K.V., Anand, P., Anilkumar, K., Rao, A.D., Prasada Rao, C.V.K. (2009). Growth and decay of Arabian Sea mini warm pool during May 2000 – Observations and simulations. *Deep Sea Res. Part I*. <http://dx.doi.org/10.1016/j.dsr.2008.12.004>.
- Huffman, G., et al. (1997). The global precipitation climatology project (GPCP) combined precipitation data set, *Bull. Am. Meteorol. Soc.*, 78, 5–20.
- Keerthi, M. G., M. Lengaigne., J. Vialard., C. de Boyer Montegut., P. M. Muraleedharan. (2013). Interannual variability of the Tropical Indian Ocean mixed layer depth, *Clim. Dyn.*, 40, 743–759.
- Keerthi, M. G., M. Lengaigne., K. Drushka., J. Vialard., C. de Boyer Montegut., S. Pous., M. Levy., P. M. Muraleedharan. (2016). Intraseasonal variability of mixed layer depth in the tropical Indian, *Clim. Dyn.*, 46(7-8), 2633–2655. doi:10.1007/s00382-015-2721-z.
- Kershaw, R. (1985). Onset of the south-west monsoon and sea-surface temperature anomalies in the Arabian Sea. *Nature* 315:561–563.
- Kershaw, R. (1988). Effect of a sea surface temperature anomaly on a prediction of the onset of the southwest monsoon over India. *Quart J R Meteor Soc* 114:325–345.
- Krishnamohan, K.S., Vialard, J., Lengaigne, M., Masson, S., Samson, G., Pous, S., Neetu, S., Durand, F., Shenoi, S.S.C., Madec, G. (2019). Is there an effect of Bay of Bengal salinity on the northern Indian Ocean climatological rainfall? *Deep-Sea Res. II*. <https://doi.org/10.1016/j.dsr2.2019.04.003>.
- Kurian, J., & Vinayachandran, P. N. (2007). Mechanisms of formation of the Arabian Sea mini warm pool in a high - resolution ocean general circulation model. *Journal of Geophysical Research Oceans*, C05009 112(5), 1–14. <https://doi.org/10.1029/2006JC003631>.
- Locarnini, R. A., A. V. Mishonov., J. I. Antonov., T. P. Boyer., H. E. Garcia., O. K. Baranova., M. M. Zweng., D. R. Johnson. (2010). World Ocean Atlas, 2009, vol. 1, in NOAA Atlas NESDIS 68, edited by T. S. Levitus, U.S. Gov. Print. Off., Washington, D. C.
- Lukas, R., & Lindstrom, E. (1991). The mixed layer of the western equatorial Pacific Ocean. *Journal of Geophysical Research: Oceans*, 96(S01), 3343-3357.
- Madec, G. (2008). NEMO ocean engine, Note Pôle Modél. 27, Inst. Pierre- Simon Laplace, Paris.

- Masson, S., Luo, J.J., Madec, G., Vialard, J., Durand, F., Gualdi, S., Guilyardi, E., Behera, S., Delécluse, P., Navarra, A. and Yamagata, T. (2005). Impact of barrier layer on winter–spring variability of the southeastern Arabian Sea. *Geophys. Res. Lett.* 32, L07703. doi:10.1029/2004GL021980p.
- Mathew, S., Natesan, U., Latha, G., & Venkatesan, R. (2018). Dynamics behind warming of the southeastern Arabian Sea and its interruption based on in situ measurements. *Ocean Dynamics*, 68(4-5), 457-467.
- Meissner, T., Wentz, F., Le Vine, D. (2018). The salinity retrieval algorithms for the NASA Aquarius version 5 and SMAP version 3 releases. *Remote Sens.* 10 (7), 1121.
- Murtugudde, R., McCreary, J. P., Busalacchi, A. J. (2000). Oceanic processes associated with anomalous events in the Indian Ocean with relevance to 1997–1998. *J Geophys Res* 105:3295–3306.
- Neema, C. P., Hareeshkumar, P. V., Babu, C. A. (2012). Characteristics of Arabian Sea mini warm pool and Indian summer monsoon. *Climate Dynamics*, 38(9–10), 2073–2087. <https://doi.org/10.1007/s00382/011/1166/2>
- Nisha, K., M. Lengaigne, V. V. Gopalakrishna, J. Vialard, S. Pous, A. C. Peter, F. Durand, S. Naik. (2013). Processes of summer intraseasonal sea surface temperature variability along the coasts of India, *Ocean Dyn.*, 63, 329–346.
- Nyadjro, E. S., Subrahmanyam, B., Murty, V. S. N., & Shriver, J. F. (2012). The role of salinity on the dynamics of the Arabian Sea mini warm pool. *Journal of Geophysical Research Oceans*, C09002117(9), 1–12. <https://doi.org/10.1029/2012JC007978>.
- Nyadjro, E. S., Subrahmanyam, B. (2014). SMOS satellite mission reveals the salinity structure of the Indian Ocean Dipole. *IEEE Geosci Remote Sens Lett* 11:1564–1568.
- Pant, V., M. S. Girishkumar., T. V. S. Udaya Bhaskar., M. Ravichandran., F. Papa., V. P. Thangaprakash. (2015). Observed interannual variability of near-surface salinity in the Bay of Bengal, *J. Geophys. Res. Oceans*, 120, 3315–3329, doi:10.1002/2014JC010340.
- Papa, F., F Durand., A. Rahman., S. K. Bala., W. B. Rossow. (2010). Satellite altimeter-derived monthly discharge of the Ganga-Brahmaputra River and its seasonal to interannual variations from 1993 to 2008, *J. Geophys. Res.* 115 C12013 doi: 10.1029/2009JC006075.
- Papa, F., Bala, S. K., Pandey, R. K., Durand, F., Gopalakrishna, V. V., Rahman, A., Rossow, W. B. (2012). Ganga–Brahmaputra river discharge from Jason-2 radar altimetry: an update to the long-term satellite-derived estimates of continental freshwater forcing flux into the Bay of Bengal. *J. Geophys. Res.* 117, C11021. <http://dx.doi.org/10.1029/2012JC008158>.
- Prasanna Kumar, S., et al. (2004). Intrusion of the Bay of Bengal water into the Arabian Sea during winter monsoon and associated chemical and biological response, *Geophys. Res. Lett.*, 31, L15304, doi:10.1029/2004GL020247.
- Praveen Kumar, B., J. Vialard., M. Lengaigne., V. S. N. Murty., M. J. McPhaden. (2012). TropFlux: Air-sea fluxes for the global tropical oceans—description and evaluation against observations, *Clim. Dyn.*, 38, 1521–1543.

- Praveen Kumar, B., J. Vialard., M. Lengaigne., V. S. N. Murty., G. R. Foltz., M. J. McPhaden., S. Pous., C. de Boyer Montegut. (2014). Processes of interannual mixed layer temperature variability in the thermocline ridge of the Indian Ocean, *Clim. Dyn.*, 43, 2377, doi:10.1007/s00382-014-2059-y.
- Rao, K. G., & Goswami, B. N. (1988). Interannual variations of sea surface temperature over the Arabian Sea and the Indian monsoon: A new perspective. *Monthly Weather Review*, 116(3), 558-568.
- Rao, R. R., Sivakumar, R. (1999). On the possible mechanism of the evolution of a mini-warm pool during the pre-summer monsoon season and the genesis of onset vortex in the south-eastern Arabian Sea. *Q J R Meteorol Soc* 125(555):787–809. <https://doi.org/10.1002/qj.49712555503>.
- Rao, R. R., and R. Sivakumar. (2003). Seasonal variability of sea surface salinity and salt budget of the mixed layer of the north Indian Ocean, *J. Geophys. Res.*, 108(C1), 3009, doi:10.1029/2001JC00907.
- Rao, R. R., Jitendra, V., GirishKumar, M. S., Ravichandran, M., & Ramakrishna, S. S. V. S. (2015). Interannual variability of the Arabian Sea Warm Pool: observations and governing mechanisms. *Climate Dynamics*, 44(7), 2119-2136.
- Rao, R. R., & Ramakrishna, S. S. V. S. (2017). Observed seasonal and interannual variability of the near-surface thermal structure of the Arabian Sea Warm Pool. *Dynamics of Atmospheres and Oceans*, 78, 121-136.
- Saji, N. H., B. N. Goswami., P. N. Vinayachandran., T. Yamagata. (1999). A dipole mode in the tropical Indian Ocean, *Nature*, 401(6751), 360–363.
- Samson, G., Masson, S., Lengaigne, M., Keerthi, M.G., Vialard, J, Pous, S., Madec, G., Jourdain, N.C., Jullien, S., Menkes, C., Marchesiello, P. (2014). The NOW regional coupled model: Application to the tropical Indian Ocean climate and tropical cyclone activity. *J. Adv. Model. Earth Syst.* 6, 700-722. doi:10.1002/2014MS000324.
- Sanilkumar, K. V., Hareesh Kumar, P.V., Joseph, J. K., Panigrahi, J. K. (2004). Arabian Sea mini warm pool in the eastern Arabian Sea during May 2000. *Curr Sci.* 86:180–184.
- Seetharamayya, P. and Master, A. (1984). Observed air-sea interface conditions and a monsoon depression during MONEX-1979. *Arch Meteorol Geophys Bioclimatol.* 33:61–67.
- Sengupta, D., Ray, P. K., Bhat, G. S. (2002). Spring warming of the eastern Arabian Sea and Bay of Bengal from buoy data. *Geophysical Research Letters*, 29(15), 24-1.
- Shankar, D., & Shetye, S. R. (1997). On the dynamics of the Lakshadweep high and low in the southeastern Arabian Sea. *Journal of Geophysical Research: Oceans*, 102(C6), 12551-12562.
- Shenoi, S. S. C., Shankar, D., Shetye, S. R. (1999). On the sea surface temperature high in the Lakshadweep Sea before the onset of the southwest monsoon. *Journal of Geophysical Research Oceans*, 104(C7), 15703–15712. <https://doi.org/10.1029/1998jc900080>.
- Skamarock, W. C., Klemp, J. B. (2008). A time-split nonhydrostatic atmospheric model for weather research and forecasting applications. *J Comput Phys.* 227(7):3465–3485. <https://doi.org/10.1016/j.jcp.2007.01.037>.

- Subrahmanyam, B., Murty, V. S. N., Heffner, D. M. (2011). Sea surface salinity variability in the tropical Indian Ocean. *Remote Sens Environ* 115:944–956.
- Sudre, J., Maes, C., Garçon, V. (2013). On the global estimates of geostrophic and Ekman surface currents. *Limnol. Oceanogr: Fluids Environ.* 3 (1), 1–20.
- Suresh, I., Vialard, J., Izumo, T., Lengaigne, M., Han, W., Mc- Creary, J., Muraleedharan, P. M. (2016). Dominant role of winds near Sri Lanka in driving seasonal sea-level variations along the west Indian coast, *Geophys. Res. Lett.*, 43, 7028–7035, doi:10.1002/2016GL069976.
- Suresh, I., Vialard, J., Lengaigne, M., Izumo, T., Parvathi, V., Muraleedharan, P.M. (2018). Sea level interannual variability along the west coast of India. *Geophys. Res. Lett.* 45 (22), 12–440.
- Thadathil, P. and Gosh, A. K. (1992). Surface layer temperature inversion in the Arabian Sea during winter. *J Oceanogr.* 48(3):293–304. <https://doi.org/10.1007/BF02233989>.
- Thadathil. P., Thoppil, P., Rao, R. R., Muralidharan, P. M., Somayajulu, Y. K., Gopalakrishna, V. V., Murtugudde, R., Reddy, G. V., Revichandran, C. (2008). Seasonal variability of the observed barrier layer in the Arabian Sea. *J Phys Oceanogr.* 38(3):624–638. <https://doi.org/10.1175/2007JPO3798.1>
- Vialard, J., K. Drushka., H. Bellenger., M. Lengaigne., S. Pous., J. P. Duvel. (2013). Understanding Madden-Julian-Induced Sea surface temperature variations in the North Western Australian Basin, *Clim. Dyn.* 41, 3203–3218.
- Vialard, J., & Delecluse, P. (1998). An OGCM study for the TOGA decade. Part I: Role of salinity in the physics of the western Pacific fresh pool. *Journal of Physical Oceanography*, 28(6), 1071-1088.
- Vinayachandran, P.N., Shankar, D., Kurian, J., Durand, F., Shenoi, S.S.C. (2007). Arabian Sea mini warm pool and the monsoon onset vortex. *Current Sci.* 93(2), 203-214.

Figures

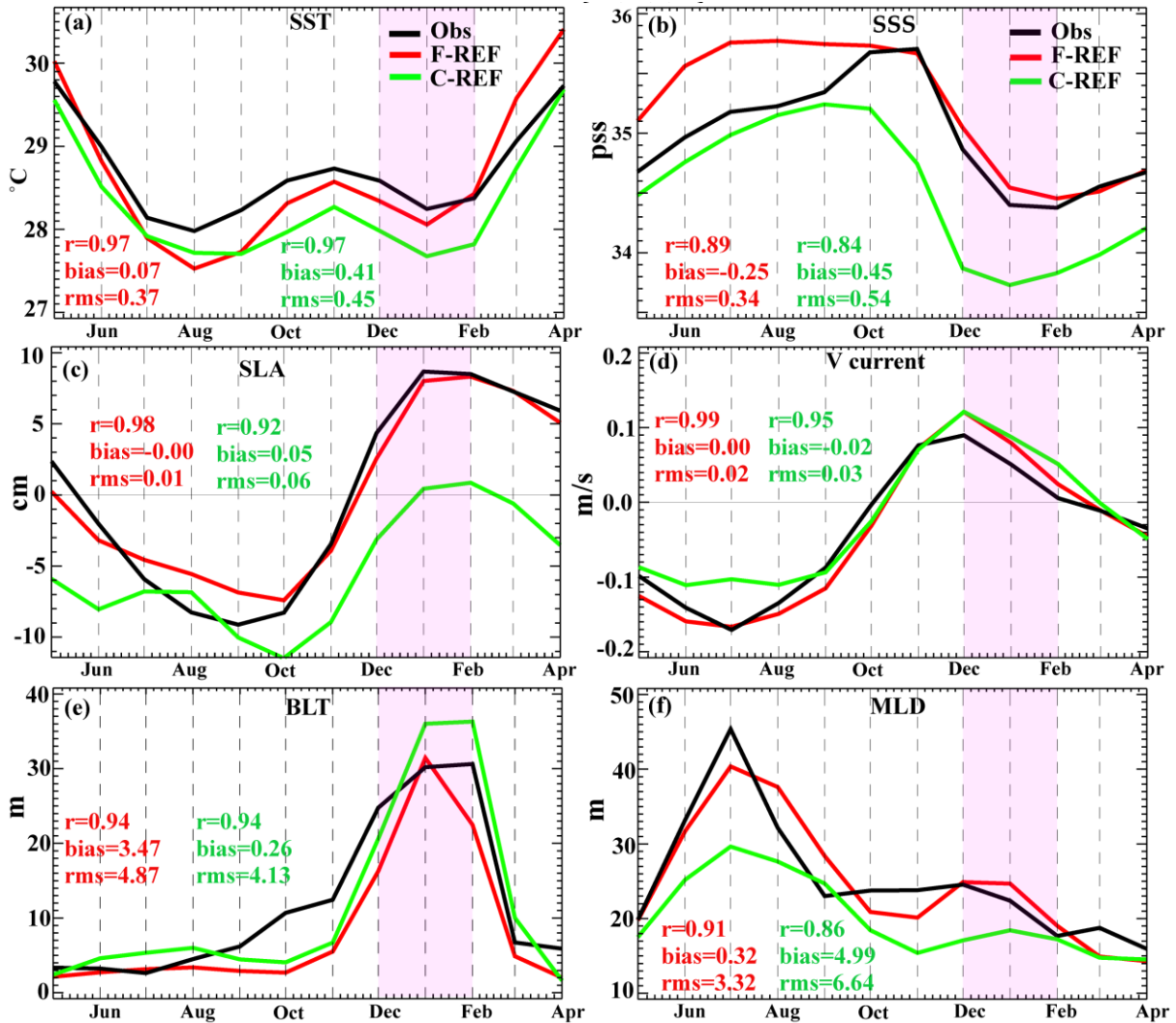


Figure 1: Seasonal evolution of (a) SST, (b) SSS, (c) SLA, (d) Meridional current, (e) BLT and (f) MLD averaged over the SEAS box (70-77 $^{\circ}$ E, 5-12 $^{\circ}$ N: red frames on the figure 2) from May to April for F-REF experiment (red), C-REF experiment (green) and Observations (Black). The correlation (r), bias and root mean square difference (rms) of F-REF experiment (in red color) and C-REF experiment (in green color) to observations are given in each panel. Observed climatologies are obtained from the NOAA OI SST (a), ESA Climate Change Initiative (CCI) SSS product (b), AVISO merged sea level (c), GECKO surface current estimates (d), de Boyer Montegut et al. (2004) climatology (e,f): see section 2.3 for more details.

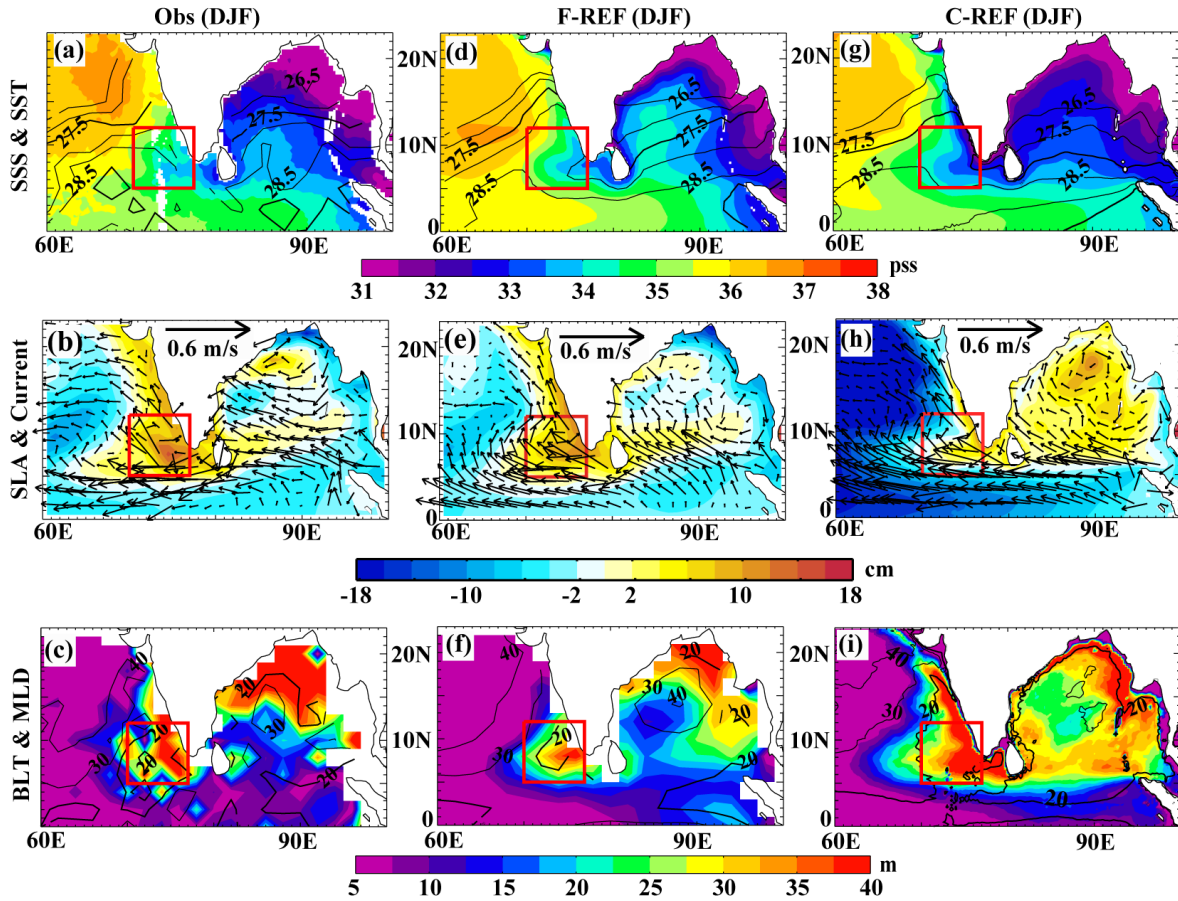


Figure 2: Winter (December-January-February) climatological maps for (a, d, g) SSS (color) and SST (contour), (b, e, h) SLA (color) and surface current (vectors), (c, f, i) BLT (color) and MLD (contour) in the Northern Indian Ocean. From (left) Observations, Forced model (F-REF, middle) and Coupled model (C-REF, right).

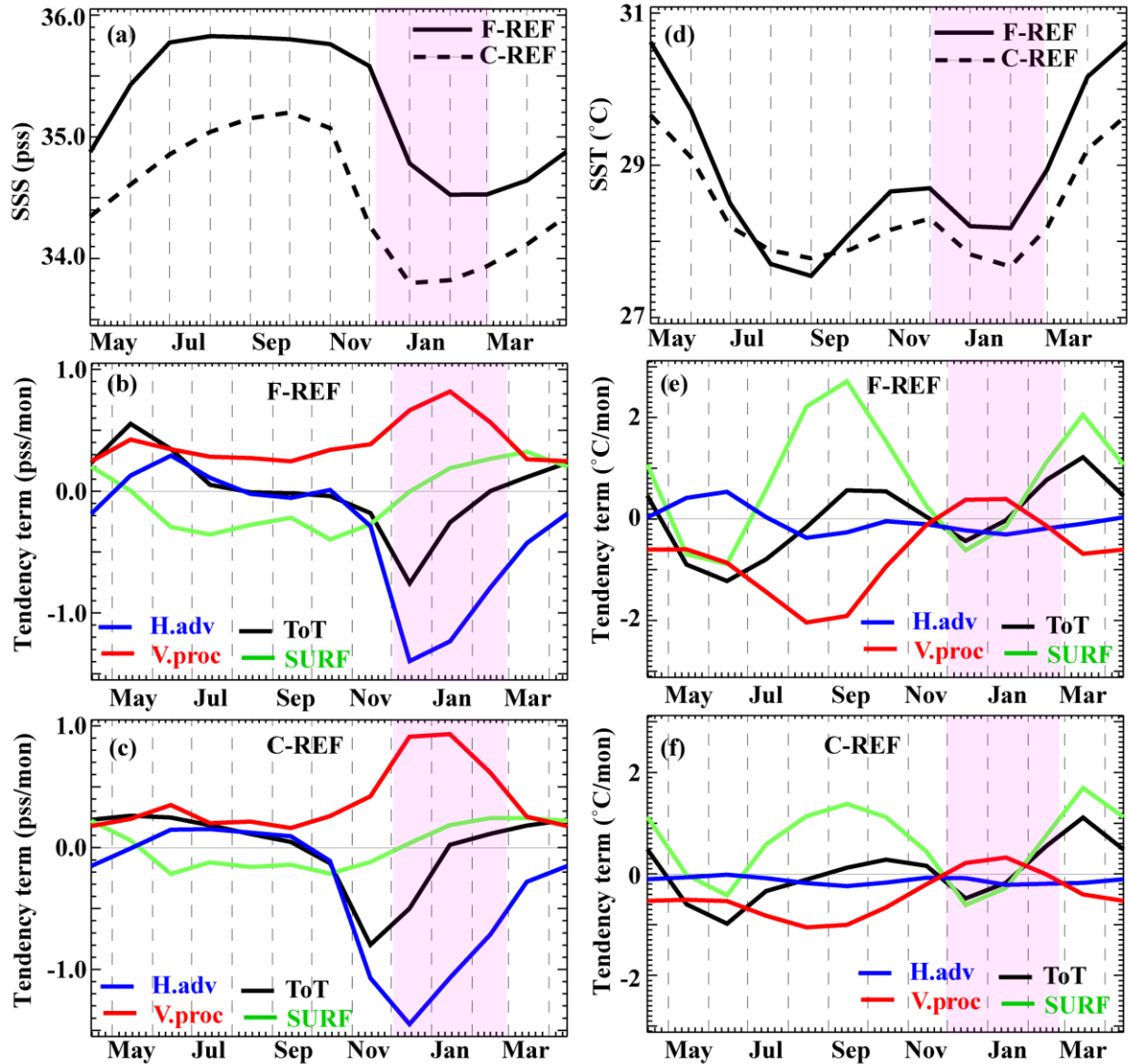


Figure 3: SEAS box (red frames on figure 2) average climatological seasonal cycle for (a) mixed layer salinity in F-REF (continuous line) and C-REF (dashed line), and mixed layer salinity tendency terms (pss month^{-1} , horizontal advection in blue, vertical process in red, surface freshwater forcing in green, and total tendency in black) for (b) F-REF and (c) C-REF. (d) mixed layer temperature in F-REF (continuous line) and C-REF (dashed line), and mixed layer temperature tendency terms ($^{\circ}\text{C month}^{-1}$, horizontal advection in blue, vertical process in red, surface heat flux forcing in green, and total tendency in black) for (e) F-REF and (f) C-REF. Pink band highlight represents 1 December to 28 February.

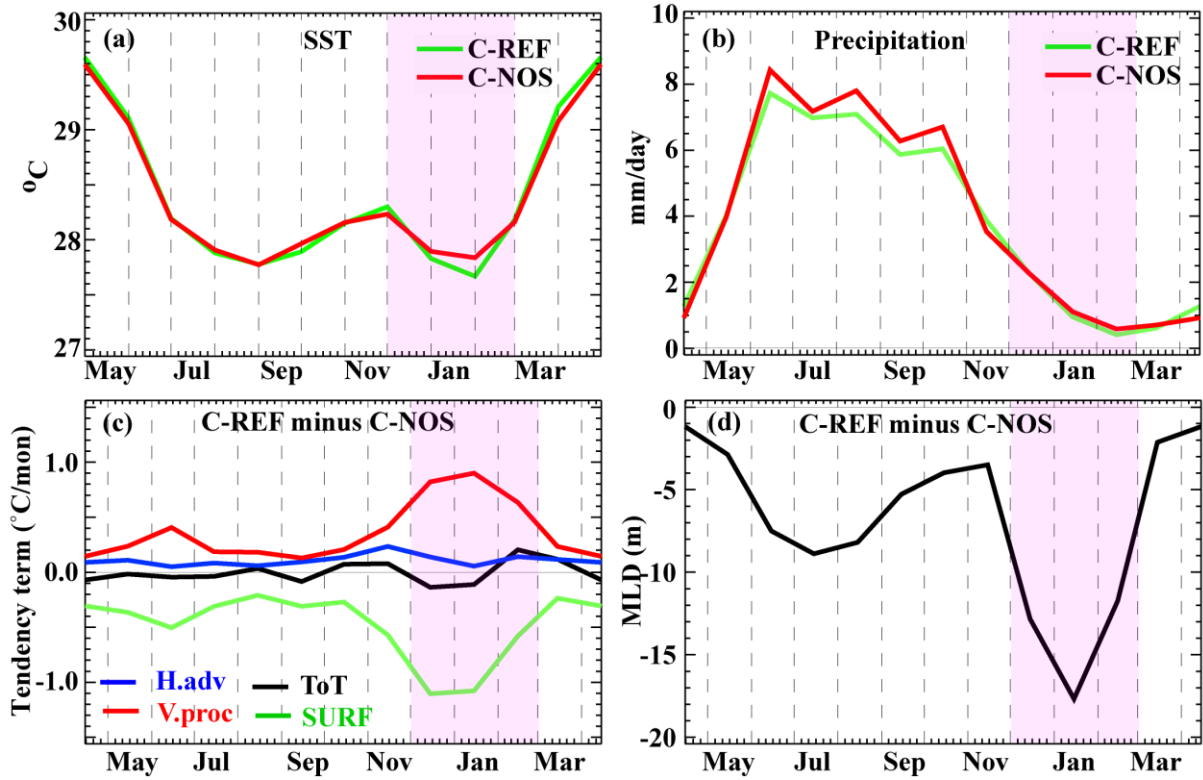


Figure 4: Climatological seasonal cycle averaged over the SEAS box (red frames on figure 2) for (a) SST and (b) Precipitation of C-REF (green) and C-NOS (red); and of (c) mixed layer heat budget terms ($^{\circ}\text{C month}^{-1}$, horizontal advection in blue, vertical process in red, surface heat flux forcing in green, and total tendency in black) and (d) MLD (m) for C-REF minus C-NOS. Pink band highlight represents 1 December to 28 February.

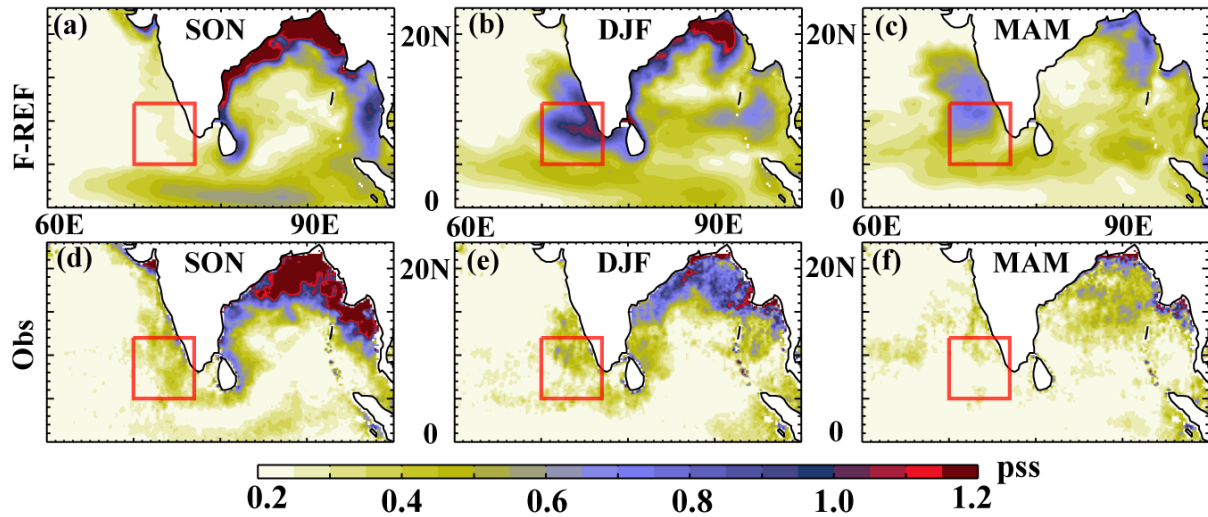


Figure 5: Standard deviation of SSS interannual anomalies (SSS') in the F-REF experiment for (a) September-November (SON), (b) December-February (DJF), (c) March-May (MAM). (d to f) As (a-c) but for CCI+SSS (2010 to 2019).

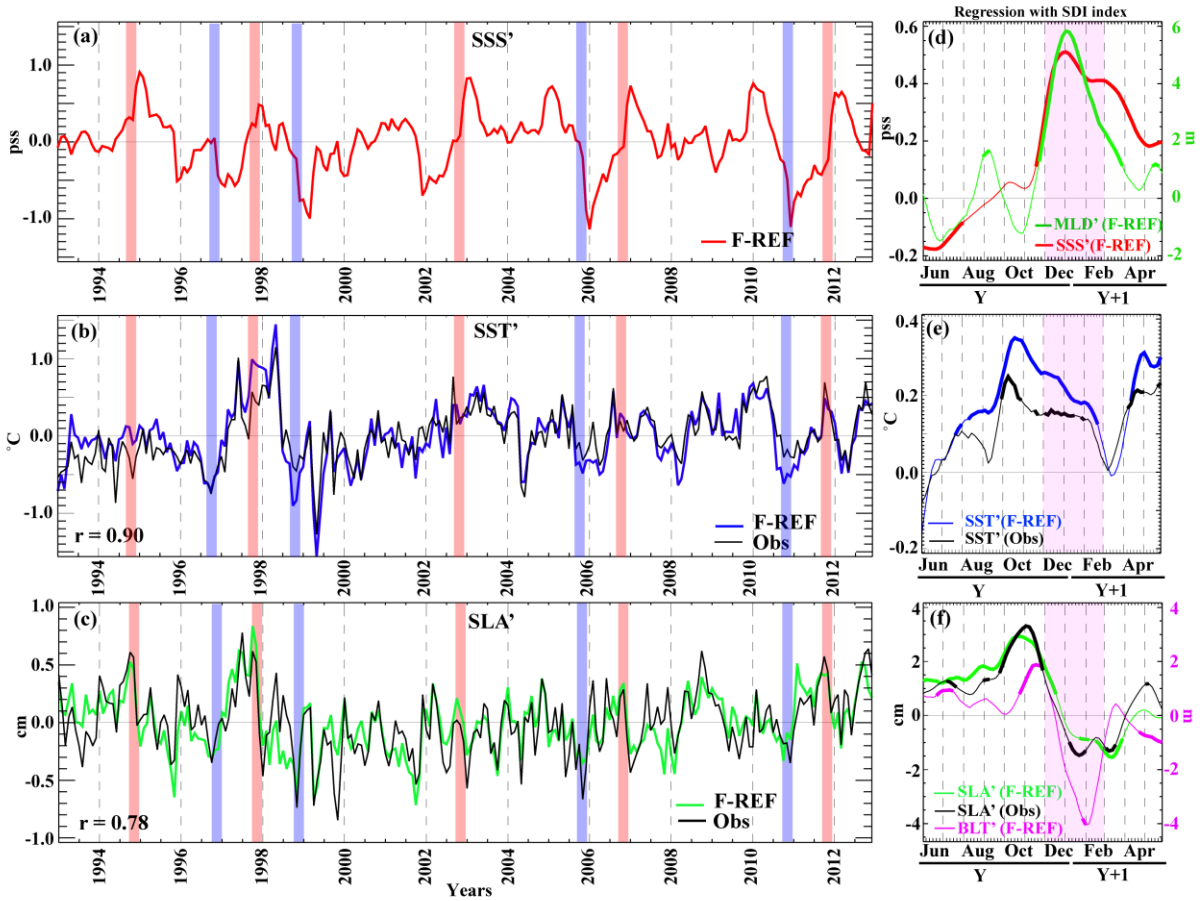


Figure 6: Average SEAS (red frames on figure 2) timeseries of interannual anomalies of (a) SSS, (b) SST and (c) SLA for F-REF experiment (colored lines) and SST and SLA observations (black lines). Blue (red) shade marks the SON period during negative (positive) IOD years. Lead-lag regression onto the normalized September-November (SON) SDI (Sea level anomaly based Indian ocean Dipole Index) for (d) F-REF SSS interannual anomaly (Red line) and MLD interannual anomaly (green line), (e) SST interannual anomaly (Blue line for F-REF and Black line for Observation), (f) SLA interannual anomaly (Green line for F-REF and black line for Observation) and BLT interannual anomaly (Magenta line for F-REF). Thick lines on panels d, e, f indicate signals that are different from zero at the 90% confidence level.

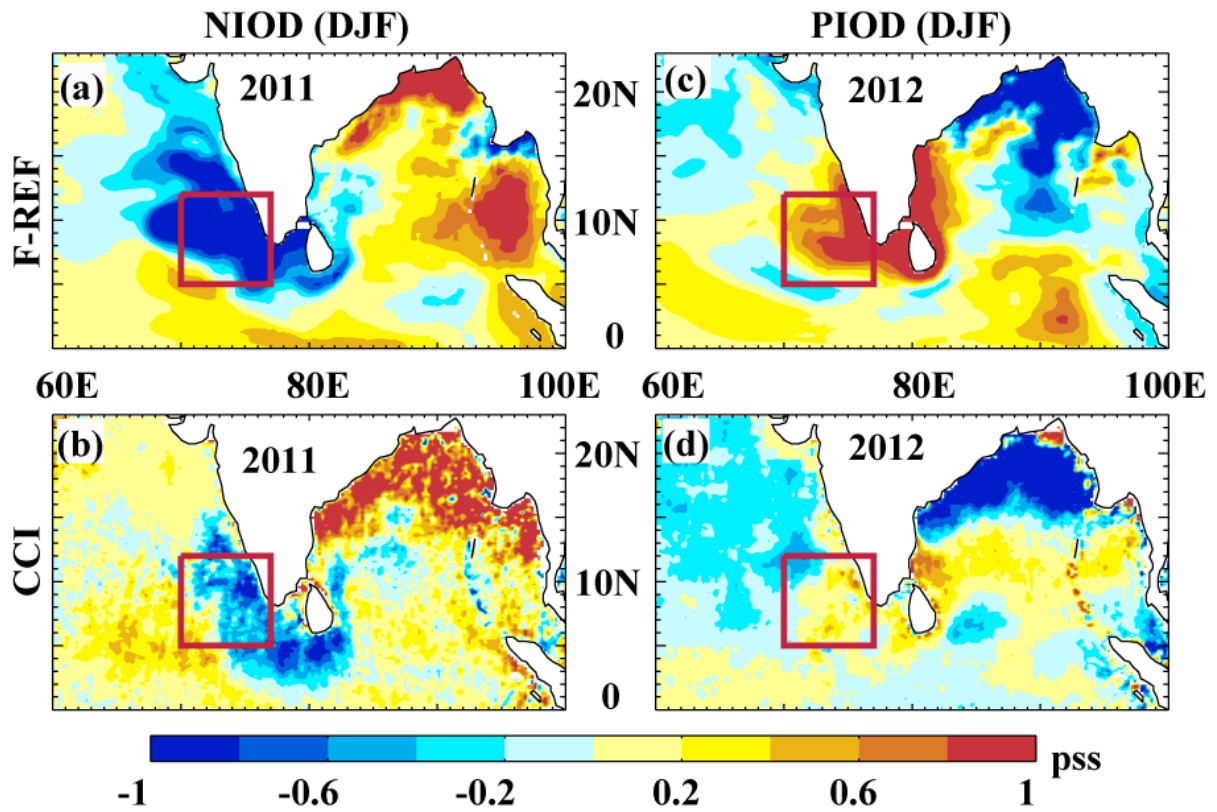


Figure 7: Average December-February sea surface salinity (SSS) anomaly in (a,b) 2011 (after the negative 2010 IOD) and (c,d) 2012 (after the positive 2011 IOD), in (a,c) F-REF and (b,d) CCI SSS remotely-sensed observations.

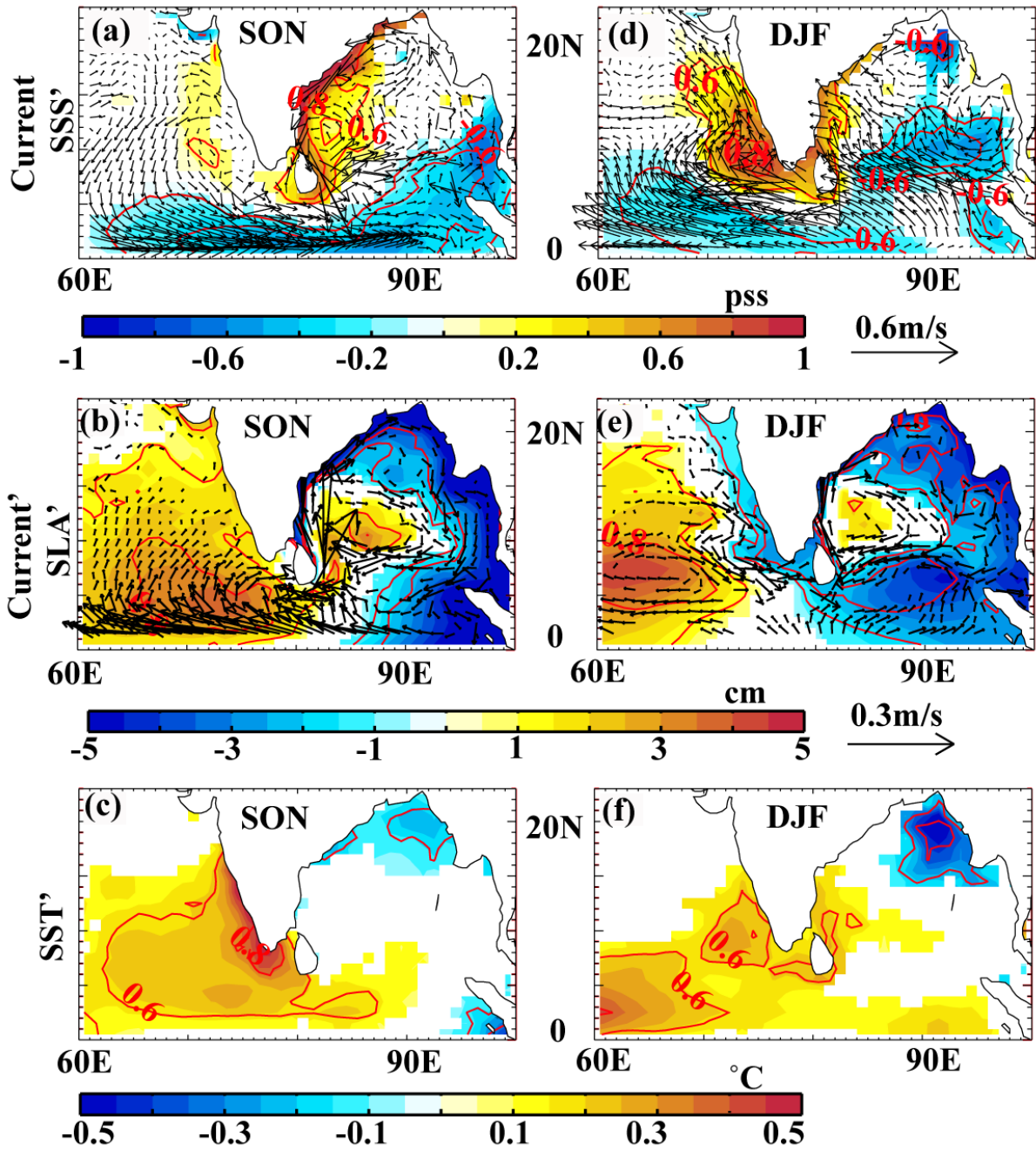


Figure 8: Regression map of SON interannual anomalies of (a) SSS (color), (b) SLA (colors) and currents (vectors) and (c) SST onto the normalized September-November (SON) SDI (Sea level anomaly based Indian ocean Dipole Index). Signals that are not significantly different from zero at the 90% confidence level are masked. The vectors on panel (a) show the SON climatological surface currents. The red contours on all panels indicate the correlation between the SON interannual anomalies of variables displayed in color and the SON average of the SDI index. (d, e, f) as (a,b,c) but for December-February average quantities, regressed onto the normalized SDI index of the previous SON.

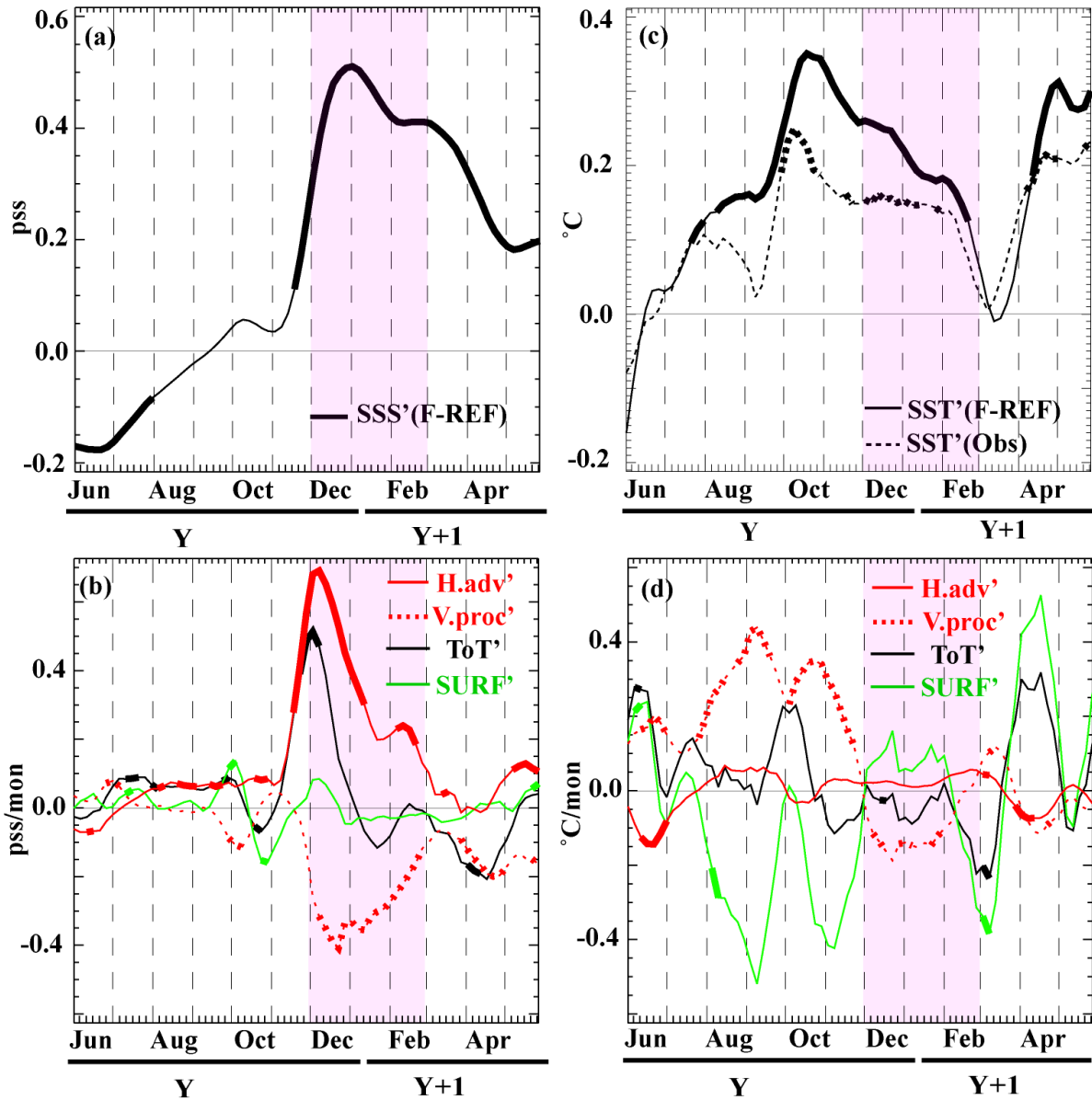


Figure 9: Lead-lag regression onto the normalized SDI-SON index for SEAS-average (a) F-REF SSS interannual anomalies SSS' (black line), (b) mixed layer salinity tendency terms interannual anomalies (pss month^{-1} , horizontal advection in blue, vertical process in red, surface freshwater forcing in green, and total tendency in black), (c) SST interannual anomalies SST' (black line for F-REF and black dashed line for observations) and (d) mixed layer temperature tendency terms interannual anomalies ($^{\circ}\text{C month}^{-1}$, horizontal advection in blue, vertical process in red, surface heat flux forcing in green, and total tendency in black). Thick lines indicate signals that are different from zero at the 90% confidence level.